# Final Technical Report on STTR Project DE-FG02-04ER86191

**Hydrogen Cryostat for Muon Beam Cooling** was an STTR project begun in July 2004 and ended in January 2008 with Muons, Inc. (Dr. Rolland Johnson, PI) and Fermi National Accelerator Laboratory (Dr. Victor Yarba, Subcontract PI) to extend the use of hydrogen in ionization cooling to that of refrigerant in addition to breakdown suppressant and energy absorber. The project was to develop cryostat designs that could be used for muon beam cooling channels where hydrogen would circulate through refrigerators and the beam-cooling channel to simultaneously refrigerate 1) high-temperature-superconductor (HTS) magnet coils, 2) cold copper RF cavities, and 3) the hydrogen that is heated by the muon beam. In an application where a large amount of hydrogen is naturally present because it is the optimum ionization cooling material, it was reasonable to explore its use with HTS magnets and cold, but not superconducting, RF cavities. In this project we developed computer programs for simulations and analysis and conducted experimental programs to examine the parameters and technological limitations of the materials and designs of Helical Cooling Channel (HCC) components (magnet conductor, RF cavities, absorber windows, heat transport, energy absorber, and refrigerant).

A consequence of this study was the demonstration that hydrogen refrigeration of super-conducting magnets is not optimum for muon cooling applications because it limits their operation to temperatures above the 14 K hydrogen freezing point. That is, in all cases that were studied, the highest possible magnetic fields for muon ionization cooling were required such that the coils had to be colder than liquid hydrogen refrigeration could provide.

One of the outstanding results of this project is that our study of HTS became the basis for initiatives and proposals to use HTS magnets operating at liquid helium temperatures for extremely high fields and more effective muon beam cooling. Another outstanding result was the invention of the Helical Solenoid (HS), a new way to create the required solenoid, helical dipole, and helical quadrupole fields of the HCC that uses a simple configuation of circular coils. The HS has become the basis for subsequent projects for six-dimensional beam cooling, the MANX demonstration experiment, and stopping muon beams for rare decay searches. The funds from this project also supported measurements of breakdown in an RF cavity pressurized with hydrogen that showed that high gradients were possible even in stong magnetic fields.

The results of the project were reported in more than a dozen published conference reports. The most significant of these are attached as appendices to this report. The project also supported the training of postdoctoral accelerator physicists, including Dr. Katsuya Yonehara, who is now a Peoples Fellow at Fermilab, and Dr. Mohammad Alsharo'a who is now employed as an accelerator engineer with Muons, Inc.

The project showed that although a hydrogen cryostat is not the optimum solution for muon ionization cooling channels, the studies of the cooling channel components that define the cryostat requirements led to fundamental advances. In particular, two new lines of promising development were opened up, regarding very high field HTS magnets and the HS concept, that have led to new proposals and funded projects. A description of the physics of muon beam cooling is presented below. The technological developments of this STTR project are then described in the main body of the report and in more detail in the Appendices.

# Hydrogen Cryostat for Muon Beam Cooling

## Table of Contents

Overview and Summary ..... 2
Introduction ..... 3
Ionization Cooling Principles ..... 4
Fundamental Limitations ..... 5
Multiple Scattering ..... 5
Emittance Exchange ..... 6
New Ionization Cooling Techniques ..... 6
Gas-filled Helical Cooling Channel (HCC) ..... 7
Momentum-dependent HCC ..... 8
Parametric Resonance Ionization Cooling ..... 8
Phase Space Repartitions ..... 8
Reverse Emittance Exchange Using Absorbers ..... 8
Muon Bunch Coalescing ..... 9
New Cooling Technology Results From This Project ..... 10
Pressurized RF Cavities ..... 10
HTS at Low Temperature ..... 11
Helical Solenoid ..... 11
High Field Superconductors ..... 11
The MANX Muon Cooling Demonstration Experiment ..... 12
Very High Fields Using HTS at Low Temperature ..... 12
Related Muons, Inc. Projects and Derivative Technologies ..... 13
References ..... 18
Appendix I: Barzi et al. HTS for HF Magnets ..... 20
Appendix II: Kashikhin et al. SC HC Systems ..... 30
Appendix III: Alsharo'a et al. N b3Sn Studies ..... 34
Appendix IV: Cummings et al., 6D Muon Cooling Experiment ..... 38
Appendix V: Kahn et al, High Field Solenoid ..... 41

# Introduction

Recently, several things have come together to reinvigorate muon collider enthusiasts: 1) There is a great interest to have a plan for a next-generation project that would continue the energy-frontier accelerator tradition in the US. 2) The uncertainties in need, cost, and siting of the International Linear Collider (ILC) have made it clear even to strong ILC supporters that a "Plan B" is prudent. 3) While impressive work has been done toward a neutrino factory based on a muon storage ring [1,2], the physics case for such a machine will have to wait for results of experiments that are just getting started. Thus there is some muon-related accelerator expertise that is available for muon collider development. 4) As discussed below, several new ideas have arisen in the last five years for six-dimensional (6D) muon beam cooling. The advantage of achieving high luminosity in a muon collider with beams of smaller emittance and fewer muons has been recognized as a great advantage for many reasons [3], including less proton driver power on target, fewer detector background issues, and relaxed site boundary radiation limitations.

Another advantage of small 6D emittance for a collider is that the cost of muon acceleration can be reduced by using the high frequency RF techniques being developed for the ILC. To the extent that muon beams can be cooled well enough, the muon collider is an upgrade path for the ILC or its natural evolution if LHC results imply that the ILC energy is too low or if its cost is too great.

Effective 6D cooling and the recirculating of muons in the same RF structures that are used for the proton driver may enable a powerful new way to feed a storage ring for a neutrino factory [4]. This would put neutrino factory and muon collider development on a common path such that a muon collider could be realized in several stages, each independently funded and driven by high-energy physics goals, e.g. a very cool stopping muon beam, neutrino factory, Higgs factory, energy frontier collider.

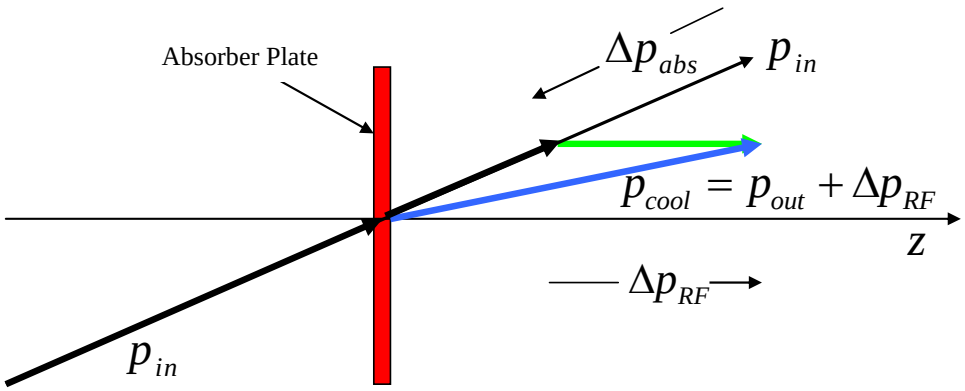


*Figure 1: Conceptual picture of the principle of Ionization Cooling. Each particle loses momentum by ionizing an energy absorber, where only the longitudinal momentum is restored by RF cavities. The angular divergence is reduced until limited by multiple scattering, so that a low-Z absorber is favored.*

**Ionization Cooling Principles**

The idea that the transverse emittance of a beam could be reduced by passing it through an energy absorber originated in Novosibirsk many years ago [5,6]. Figure 1 is a schematic of the concept, showing how the angular divergence of a beam can be reduced.

Ionization cooling of a muon beam involves passing a magnetically focused beam through an energy absorber, where the muon transverse and longitudinal momentum components are reduced, and through RF cavities, where only the longitudinal component is regenerated. After some distance, the transverse components shrink to the point where they come into equilibrium with the heating caused by multiple coulomb scattering. The equation describing the rate of cooling is a balance between these cooling (first term) and heating (second term) effects:

$$\frac{d\varepsilon_n}{ds} = -\frac{1}{\beta^2}\frac{dE_\mu}{ds}\frac{\varepsilon_n}{E_\mu} + \frac{1}{\beta^3}\frac{\beta_\perp (0.014)^2}{2E_\mu m_\mu X_0} \quad . \qquad [1].$$

Here $\varepsilon_n$ is the normalized emittance, $E_\mu$ is the muon energy in GeV, $dE_\mu / ds$ and $X_0$ are the energy loss and radiation length of the absorber medium, $\beta_\perp$ is the transverse beta-function of the magnetic channel, and $\beta$ is the normalized particle velocity. Muons passing through an absorber experience energy and momentum loss due to collisions with electrons. The derivations and discussions of the basic formulae of ionization cooling can be found in many places [7,8], where the energy loss is described by the Bethe-Bloch theory and the multiple-scattering heating is described by the Moliere theory [9].

Setting the heating and cooling terms equal defines the equilibrium emittance, the very smallest possible with the given parameters:

$$\varepsilon_n^{(equ.)} = \frac{\beta_\perp (0.014)^2}{2\beta m_\mu \frac{dE_\mu}{ds} X_0} \quad . \qquad [2].$$

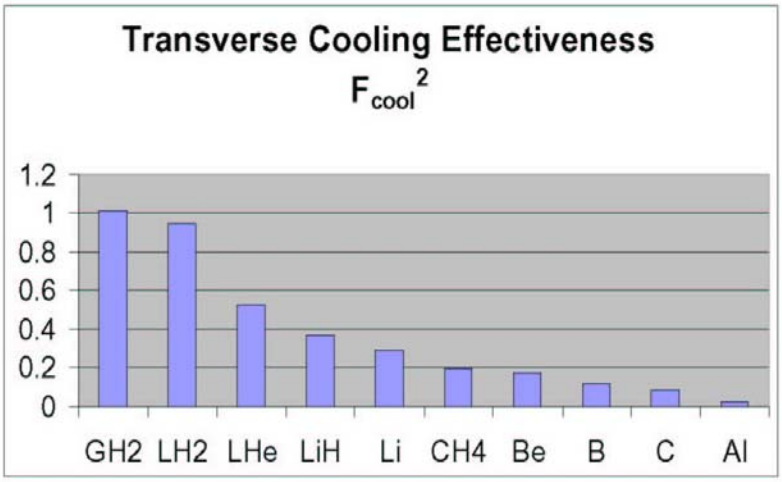


*Figure 2: A comparison of the cooling figure of merit for light materials. The equilibrium beam emittance in each transverse plane is inversely proportional to the product of the energy loss and the radiation length. The graph indicates the total figure of merit.*

A cooling factor ($F_{cool} = X_0 dE_\mu / ds$) can be uniquely defined for each material, and since cooling takes place in each transverse plane, the figure of merit is $F_{cool}^2$. For a particular

material, $F_{cool}$ is independent of density, since energy loss is proportional to density, and radiation length is inversely proportional to density. The inverse of $F_{cool}^2$ corresponds to the best equilibrium emittance that can be achieved. Superconducting solenoid focusing is used to give a value of $\beta_\perp$ as low as 10 cm. Figure 2 shows $F_{cool}^2$ for many materials of interest.

Gaseous hydrogen is the very best material that one can use from the standpoint of the final equilibrium emittance. Also, since the exponential cooling rate depends on the difference between the initial and final emittances, it provides the very best cooling rate.

**Fundamental Limitations**

The transverse beta function, $\beta_\perp$, is proportional to the ratio of momentum divided by the magnetic field. So the lowest equilibrium emittance requires the lowest momentum and the highest field.

As implied by the Bethe-Bloch equation and shown on figure 3, the fact that *dE/dx* increases as the momentum decreases means that once the momentum is below a few hundred MeV/c, any transverse cooling is necessarily accompanied by longitudinal heating. To a certain extent, this unwanted heating can be mitigated by modifying the dispersion function [10] and/or changing the profile of an absorber with shaped edges.

The maximum magnetic field is a technological problem that discussed below. One solution is the use of HTS magnets for large fields at low temperatures.

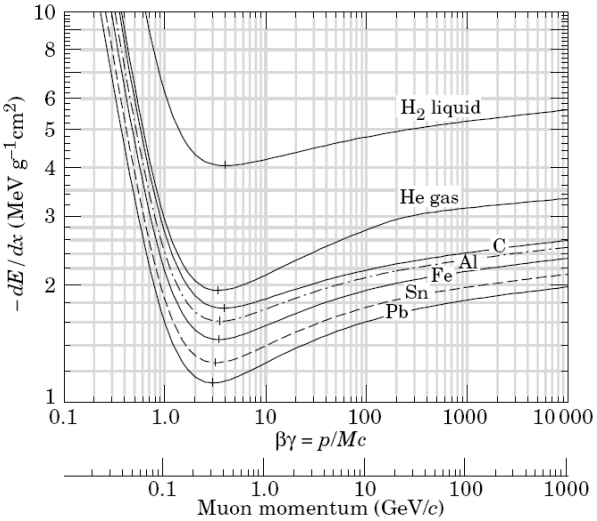


*Figure 3: Energy loss for muons in various materials taken from the Particle Data Group [11], where the minimum dE/dx for hydrogen occurs near 300 MeV/c.*

**Multiple Scattering**

Investigations of the deficiencies of the Moliere theory for low-Z materials [12] and other models [13] have been vindicated by recent measurements, as shown in figure 4. These seemingly small differences in the tails of the scattering distributions can have large consequences for long cooling channels. An ICOOL investigation indicated that as much as a factor of 3 improvement in cooling factor could be achieved with scattering models that agreed with the MuScat [14] data compared to the Geant4 models that we have used up to now.

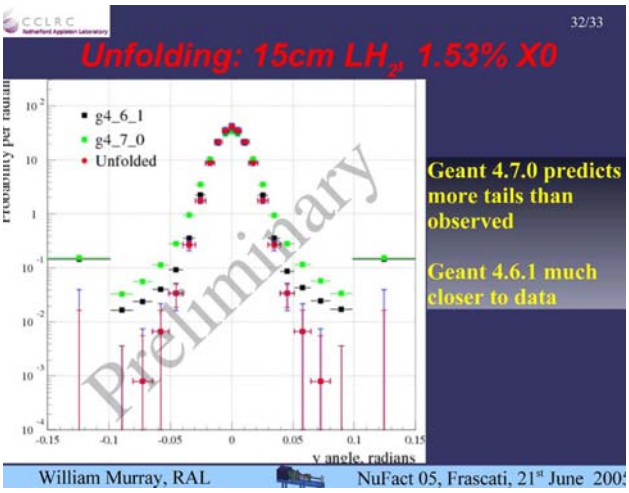


*Figure 4: Comparison of angular distributions of the MuScat experiment for muons scattering off of hydrogen with two different releases of the Geant4 simulation program. The (red) experimental data show smaller tails.*

**Emittance Exchange**

To achieve longitudinal cooling requires emittance exchange with transverse oscillations. Emittance exchange, in turn, requires the introduction of a beam bend that creates dispersion, a correlation between the orbit and energy of a particle. Figure 5 shows the conceptual pictures of the two approaches that have recently been studied most. In the left of figure 5 the use of a wedge absorber is shown, where the beam is dispersed across a wedge of energy-absorbing material such that higher momentum particles lose more energy. The muons become more monoenergetic after they pass through the wedge, while the transverse emittance is increased as part of the emittance exchange process.

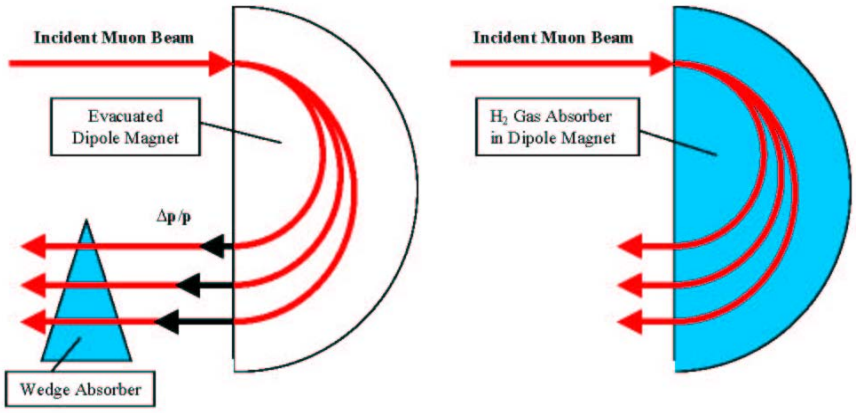


*Figure 5: Emittance exchange. LEFT: Wedge Absorber Technique. RIGHT: Homogeneous Absorber Technique where dispersion causes higher energy particles to have longer path length and thus more ionization energy loss.*

The diagram on the right of figure 5 was an invention first described in an SBIR proposal that led to the development of the HCC with a continuous absorber.

# New Ionization Cooling Techniques

**Gas-filled Helical Cooling Channel (HCC)**

The HCC is an attractive example of a cooling channel based on this idea of energy loss dependence on path length in a continuous absorber. One version of the HCC uses a series of high-gradient RF cavities filled with dense hydrogen gas, where the cavities are in a magnetic channel composed of a solenoid field with superimposed helical transverse dipole and quadrupole fields [15,16]. In this scheme, energy loss, RF energy regeneration, emittance exchange, and longitudinal and transverse cooling happen simultaneously.

The helical dipole magnet creates an outward radial force due to the longitudinal momentum of the particle while the solenoid magnet creates an inward radial force due to the transverse momentum of the particle, or

$$\begin{aligned} F_{h-dipole} &\approx p_z \times B_\perp; \quad b \equiv B_\perp \\ F_{solenoid} &\approx -p_\perp \times B_z; \quad B \equiv B_z \end{aligned},$$

where $B$ is the field of the solenoid, the axis of which defines the $z$ axis, and $b$ is the field of the transverse helical dipole at the particle position. By moving to the rotating frame of the helical fields, a time and z-independent Hamiltonian can be formed to derive the beam stability and cooling behavior [17]. The motion of particles around the equilibrium orbit is shown schematically in figure 6.

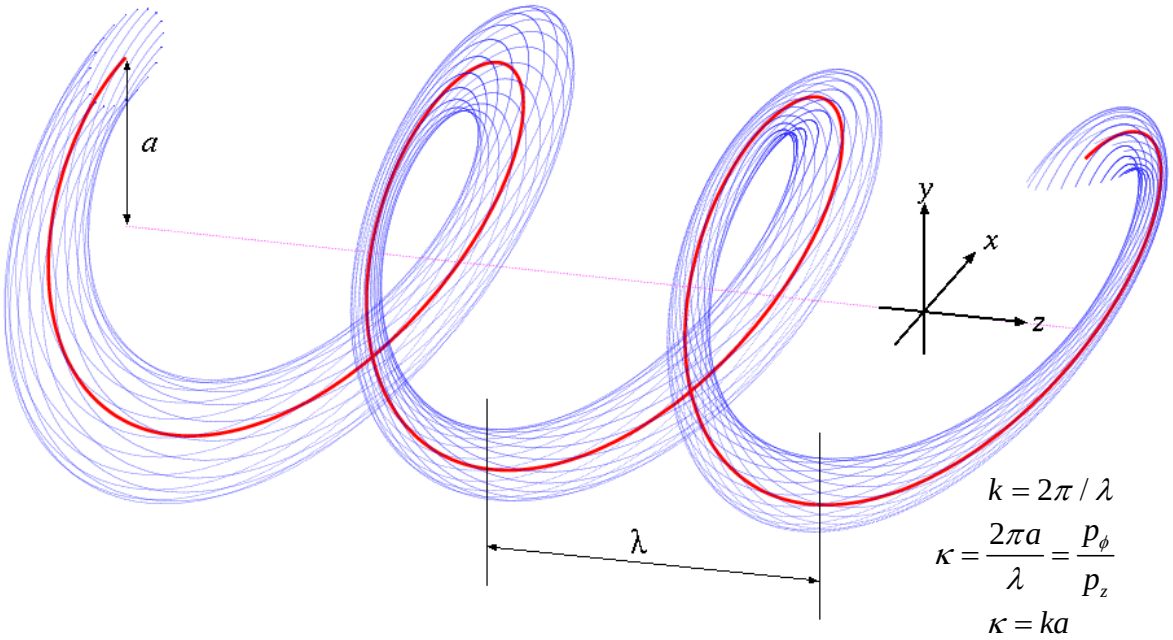


*Figure 6: Schematic of beam motion in a helical cooling channel. The equilibrium orbit shown in red follows the equation that is the Hamiltonian solution:*

$$p(a) = \frac{\sqrt{1+\kappa^2}}{k}\left[B - \frac{1+\kappa^2}{\kappa} b\right].$$

Use of a continuous homogeneous absorber as shown on the right side of figure 5, rather than wedges at discrete points, implies a positive dispersion along the entire cooling path, a condition that has been shown to exist for an appropriately designed helical dipole channel. We have also shown that this condition is compatible with stable periodic orbits. The simple idea that emittance exchange can occur in a practical homogeneous absorber without shaped edges followed from the observation that RF cavities pressurized with a low Z gas are possible [18,19].

The analytic relationships derived from this analysis were used to guide simulations using a code developed based on the GEANT4 [20] program called G4Beamline [21] and also using ICOOL [22] developed at BNL. Simulation results [10] show cooling factors or 50,000 for a series of 4 250 MeV/c HCC segments, where the magnet diameters are decreased and fields are increased as the beam cools. In this example the final field would be 17 T with a hydrogen gas pressure of 400 atmospheres.

**Momentum-dependent HCC**

While the HCC described above operates at constant energy, another set of applications follows from HCC designs where the strengths of the fields are allowed to change with the muon momentum. This momentum-dependent HCC concept was invented by Johnson and Yonehara in another SBIR project described below. The first application was a 6D precooler, where the beam is slowed in a liquid hydrogen absorber at the end of the pion decay channel, with 6D emittance reduction by a factor of 6. The second application is the MANX six-dimensional cooling experiment discussed below. Another application is a stopping muon beam based on a HCC [23].

**Parametric Resonance Ionization Cooling**

Parametric-resonance Ionization Cooling (PIC) [24] was invented by Derbenev and Johnson and first seen as an SBIR proposal. PIC requires a half integer resonance to be induced in a ring or beam line such that the normal elliptical motion of particles in $x - x'$ phase space becomes hyperbolic, with particles moving to smaller $x$ and larger $x'$ as they pass down the beam line. (This is very similar to the technique used for half integer extraction from a synchrotron where the hyperbolic trajectories go to small $x'$ and larger $x$ to pass the wires of an extraction septum.) Thin absorbers placed at the focal points of the channel then cool the angular divergence of the beam by the usual ionization cooling mechanism, where each absorber is followed by RF cavities. Thus in PIC the phase space area is reduced in $x$ due to the dynamics of the parametric resonance and $x'$ is reduced or constrained by ionization cooling. The basic theory of PIC is being developed to include aberrations and higher order effects. Simulations using linear channels of alternating dipoles, quadrupoles, solenoids, or HCC's are now underway [25].

## Phase Space Repartitions

**Reverse Emittance Exchange Using Absorbers**

A muon beam that is well cooled at one or two hundred MeV/c will have its unnormalized longitudinal emittance reduced by a factor of a thousand or more at 100 or more GeV collider energy. At the interaction point in the collider the bunch length would then be much shorter than the IR focal length. In reverse emittance exchange (REMEX), Derbenev proposes to repartition

the emittances to lengthen each bunch and narrow the transverse emittances using beryllium wedge energy absorbers.

Calculations show that two stages of reverse emittance exchange, one at low energy and one at a higher energy before energy straggling becomes significant, can reduce each transverse emittance by an order of magnitude.

**Muon Bunch Coalescing**

One of the newest ideas is to cool less intense bunches at low energy and to recombine them into intense bunches at higher energy where wake fields, beam loading, and space charge tune shifts are less problematic [26]. This idea was developed under an SBIR grant. Both PIC and REMEX techniques involve the focusing of a beam onto an energy absorber for which beryllium is better suited than the lower-Z materials shown in figure 2. First, the higher density of beryllium allows the thickness of the absorber to be a smaller fraction of a betatron wavelength and thereby more effective since the average betatron function in the region of the absorber is closer to the minimum value. Second, the energy straggling in the absorbers leads to longitudinal heating that must be controlled by emittance exchange. Thus the absorbers should be thin wedges made of beryllium which can easily be refrigerated to handle the heat deposition of the bright beams required by a muon collider.

## New Cooling Technology Results From This Project

**Pressurized RF Cavities**

A gaseous energy absorber enables an entirely new technology to generate high accelerating gradients for muons by using the high-pressure region of the Paschen curve [27]. This idea of filling RF cavities with gas is new for particle accelerators and is only possible for muons because they do not scatter as do strongly interacting protons or shower as do less-massive electrons. Measurements by Muons, Inc. and IIT at Fermilab have demonstrated that hydrogen gas suppresses RF breakdown very well, about a factor six better than helium at the same temperature and pressure. Consequently, much more gradient is possible in a hydrogen-filled RF cavity than is needed to overcome the ionization energy loss, provided one can supply the required RF power. Hydrogen is also twice as good as helium in ionization cooling effectiveness, viscosity, and heat capacity. Present research efforts include tests of materials in pressurized RF Cavities in magnetic fields [28] as shown in Figure 7, where an external field causes no apparent reduction in maximum achievable gradient. Crucial beam tests of the concept are scheduled in 2008.

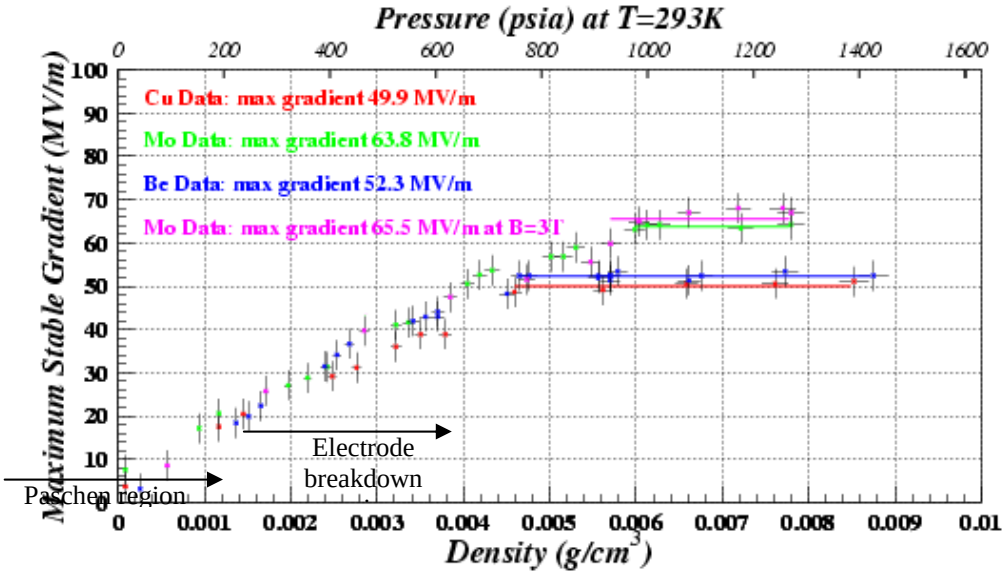


*Figure 7: Measurements of the maximum stable RF gradient as a function of hydrogen gas pressure at 805 MHz with no magnetic field for three different electrode materials: Cu (red), Mo (green), and Be (blue). The cavity was also operated at the same gradients in a 3T field with Mo electrodes (magenta).*

High-pressure RF cavities near the pion production target can be used to simultaneously capture, bunch rotate, and cool the muon beam as it emerges from the decaying pions [29]. We have started an R & D effort to develop RF cavities that will operate in the extreme conditions near a production target and an effort to simulate the simultaneous capture, phase rotation, and cooling of muons as they are created from pion decay.

While this project was initially funded as an STTR grant with IIT as Muons, Inc. and IIT as research partners (described below in the Muons, Inc. Overview), delays in the Fermilab schedule meant that those funds had been exhausted by the time the MuCool Test Area was

available to do the tests of the magnetic field dependence. Consequently, funds from this Hydrogen Cryostat grant allowed us to take the magenta data shown in figure 7, which demonstrated the ability of pressurized cavities to operate in strong magnetic fields.

**HTS at Low Temperature**

The original idea of a hydrogen cryostat was based on the concept of using new HTS magnets that would operate above 14 K in muon beam cooling channels. Muons, Inc. and our research partners in the Fermilab Technical Division started by measuring the properties of available HTS conductors [30]. This original work is reported in **Appendix I**. However, since the figure of merit for ionization cooling is the strength of the focusing magnetic field, it became clear that any convenience gained by using hydrogen as a refrigerant would come at an unacceptable price. As seen in Appendix I, the current carrying capability of the HTS at higher temperatures will reduce the maximum field, and as seen in equation [2], reduce the quality of the beam cooling.

**Helical Solenoid**

The original concept of the HCC involved a rather complex magnet with separate coils to provide the required solenoid, helical dipole, and helical quadrupole fields. Figure 8 shows a new design [31] called a Helical Solenoid (HS) which uses simple offset coils to generate the three required components. This invention was conceived and developed by funding of this STTR grant. More details, and the evolution of the idea, are described in **Appendix II**.

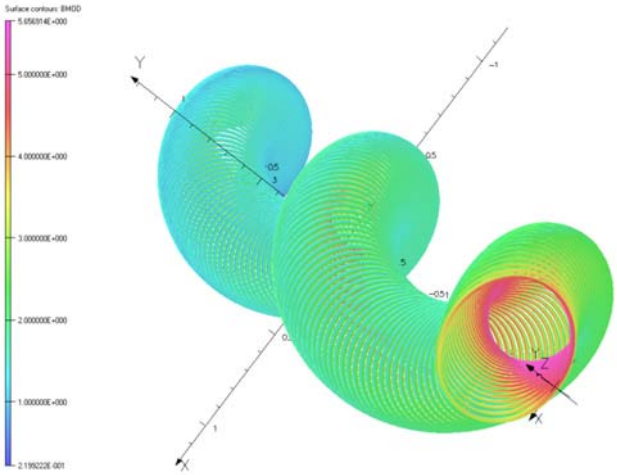

*Figure 8: Helical Solenoid geometry and flux density for the Helical Solenoid magnet for MANX.*

**High Field Superconductors**

Other low temperature superconductors are of great interest for muon cooling applications. We have also studied the use of Nb3Sn and done original research under this grant. **Appendix III** shows an ANSYS modeling effort to try to understand the manufacturing process for magnet conductors using this material.

**The MANX Muon Cooling Demonstration Experiment**

Figure 9 shows MANX, a six-dimensional muon cooling demonstration experiment based on a HCC with variable field strengths. It is being designed to slow a 300 MeV/c muon beam to about 150 MeV/c in a HCC filled with liquid helium [32]. **Appendix IV** describes the experiment, which is based on the Helical Solenoid concept.

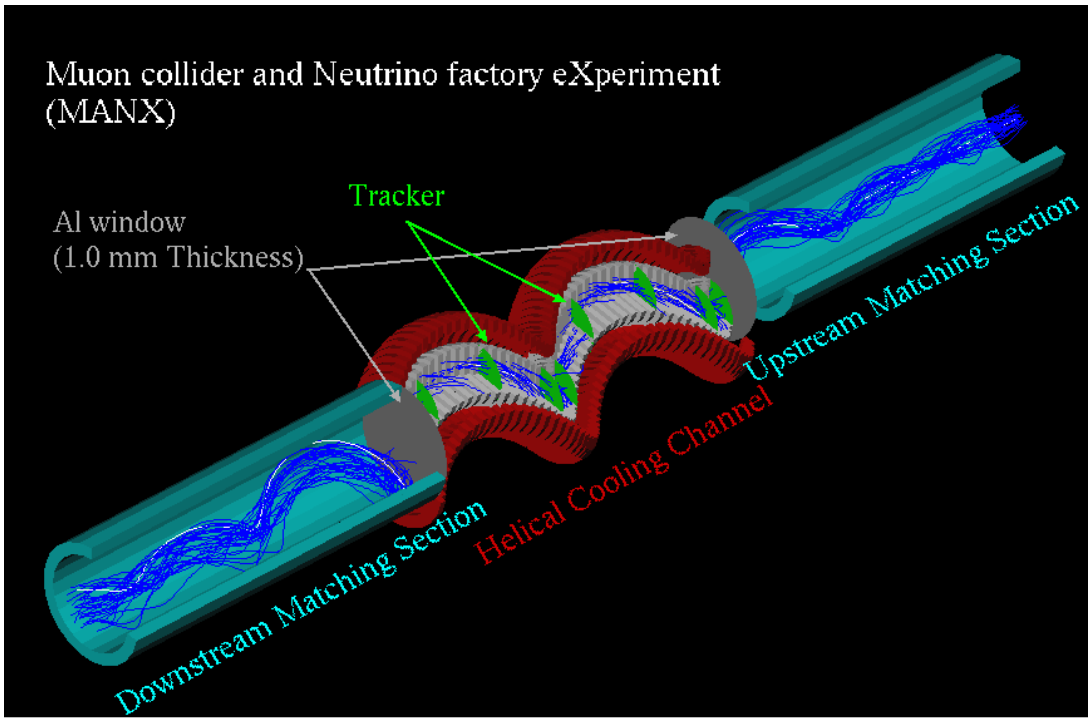


*Figure 9: Conceptual picture of the MANX apparatus. The helical solenoid magnets shown in red enclose the LHe ionization energy absorber, which is separated from the vacuum of the matching sections by thin Al windows.*

**Very High Fields Using HTS at Low Temperature**

We have learned that magnets made with HTS coils operating at low temperatures have the potential to produce extremely high fields for use in accelerators and beam lines. The specific application of interest is to use a very high field (perhaps greater than 30 Tesla) solenoid to provide a very small beta region for the final stages of cooling for a muon collider. With the commercial availability of HTS conductor based on BSCCO or YBCO technology with high current carrying capacity at 4.2 K, very high field solenoid magnets should be possible. We are evaluating the technical issues associated with building this magnet [33]. In particular we are addressing how to mitigate the high Lorentz stresses associated with this high field magnet. A paper describing this work, which is a consequence of this Hydrogen Cryostat grant, is shown in **Appendix V**. Two of the papers submitted to EPAC08 address this in more detail; abstracts are shown in **Appendix VI**.

## Related Muons, Inc. Projects and Derivative Technologies

The projects discussed below are concerned with the production, cooling, and uses of intense and bright muon beams to be used for various purposes. These SBIR and STTR projects represent a coherent, innovative program to reduce the cost of neutrino factories, facilitate designs of high-intensity muon colliders, and provide muon beams with new physics potential.

Muons, Inc. started with the idea that a gaseous energy absorber enables an entirely new technology to generate high accelerating gradients for muons by using the high-pressure region of the Paschen curve [34]. This idea of filling RF cavities with gas is new for particle accelerators and is only possible for muons because they do not scatter as do strongly interacting protons or shower as do less-massive electrons. Additionally, use of a gaseous absorber presents other practical advantages that make it a simpler and more effective beam cooling method compared to liquid hydrogen flasks in the conventional designs.

Measurements by Muons, Inc. and IIT at Fermilab have demonstrated that hydrogen gas suppresses RF breakdown very well, about a factor six better than helium at the same temperature and pressure. Consequently, much more gradient is possible in a hydrogen-filled RF cavity than is needed to overcome the energy loss, provided one can supply the required RF power. Hydrogen is also twice as good as helium in ionization cooling effectiveness, and has better viscosity and heat capacity. For these reasons hydrogen is our material of choice.

As discussed below, recent measurements taken as part of the Phase I of this proposal show that hydrogen pressurized RF cavities do not suffer from a reduction in maximum gradient while operating in intense magnetic fields as do evacuated cavities. Thus it is possible to combine the energy absorber and RF reacceleration in pressurized cavities in regions where large magnetic fields create the required focusing for ionization cooling. This means that pressurized RF cavities have two very significant advantages over any scheme involving evacuated RF cavities: greater gradient in the required magnetic field and the simultaneous use of the hydrogen gas as energy absorber and breakdown suppressant. These two advantages each lead to shorter muon cooling channel designs, which minimize the loss of muons by decay and also lower construction costs.

The use of a continuous absorber as provided by a gas-filled RF system implies a new idea (first proposed as an SBIR topic) to provide a natural, very effective means of achieving emittance exchange and true six-dimensional (6D) cooling [35]. Namely, if the superimposed magnetic field provides dispersion down the beam channel such that higher momentum corresponds to longer path length and larger ionization energy loss, the momentum spread can be reduced. Simulations of a Helical Cooling Channel (HCC) of superimposed helical dipole, helical quadrupole, and solenoid fields show a 6D emittance reduction by a factor of 50,000 in a channel only 160 meters long. This cooling factor is very much larger than in other cooling channels of comparable length.

Once the beam has been cooled in the HCC, other cooling techniques are possible. Recent developments have indicated that special cooling channels employing parametric resonances and/or very high field magnets can produce muon beams with small enough emittance that they

can be accelerated using 1.3 GHz RF cavities. Thus we have started thinking about a muon collider using superconducting RF technology as a possible upgrade to the International Linear Collider (ILC).

One possibility that was explored at the Low Emittance Muon Collider (LEMC) Workshops held at Fermilab (http://www.muonsinc.com/mcwfeb06/) Feb 6-10, 2006 and (http://www.muonsinc.com/mcwfeb07/) Feb 11-16, 2007 was to consider the proposed Fermilab 8 GeV superconducting proton driver Linac as a triple-duty machine on the path to an energy frontier muon collider. Such a Linac could accelerate protons to produce the muons, which would then be injected into the constant velocity section of the Linac to be accelerated by recirculation for use in a muon storage ring neutrino factory. (The third duty in this case would be to act as an ILC string test.) Such a neutrino factory could be very effective for two reasons. First, the neutrino production would scale with the repetition rate of the Linac and might easily outperform other designs. Second, the acceleration cost of the neutrino factory would be borne by the other uses of the superconducting Linac and the neutrino factory cost would be incremental.

In the third annual LEMC workshop (http://www.muonsinc.com/mcwapr08/) held April 21-25, 2008 the discussion evolved to be centered on the 8-GeV Project-X linear accelerator that would replace the Fermilab Booster synchrotron. We are exploring ideas to use the Project-X Linac as a double duty machine that would accelerate protons to produce the muons as well as accelerate the muons after they have been captured and cooled.

The next step, first proposed under another SBIR grant (Reverse Emittance Exchange) with Thomas Jefferson National Accelerator Facility (JLab), described below, and explored at the first and second LEMC (http://www.muonsinc.com/mcwfeb07/) Feb 12-16, 2007 workshops, is to replace the muon storage ring of the neutrino factory with a coalescing ring to combine bunches for use in a muon collider. Such a muon coalescing ring could operate at the energy of the neutrino factory storage ring, above 20 GeV. The muon beam for the collider would then be similar to that of the neutrino factory up to the coalescing ring. This approach to a muon collider has several advantages that are very attractive. First, the development of the neutrino factory based on acceleration in the 1.3 GHz RF structures requires significant muon beam cooling so that the neutrino factory becomes an intermediate step to a collider. Second, the large single bunch intensities that a high luminosity muon collider requires are not needed at low energy where space-charge, wake fields, and beam loading are problematic.

Once the beam has been coalesced into a few high intensity bunches, recirculating Linacs using 1.3 GHz RF can accelerate them to a hundred GeV/c or more for a Higgs factory or to 2 to 3 TeV/c for an energy frontier muon collider. One of the studies of the present proposal will to be to investigate bunching techniques that are well suited for coalescing.

This path to an affordable neutrino factory and a compelling design of a muon collider has complementary projects that Muons, Inc. is pursuing with SBIR/STTR grants and proposals:

**Phase II Projects**

1) The development of Pressurized **High Gradient RF Cavities** was the subject of an STTR grant with IIT (Prof. Daniel Kaplan, Subcontract PI), which began in July 2002 and ended in September 2005. In this project, Muons, Inc. built two 805 MHz test cells (TC) and used them to measure the breakdown voltages of hydrogen and helium gases at FNAL with surface gradients up to 50 MV/m on copper electrodes. Phase II started in July 2003 to extend the measurements at Fermilab's Lab G and the MuCool Test Area (MTA) to include effects of strong magnetic fields and ionizing radiation at 805 MHz. A new test cell was built under this grant, passed safety requirements associated with the high pressure hydrogen, and was used to extend Paschen curve measurements for hydrogen beyond 60 MV/m surface gradient (20μs pulse width) using electropolished molybdenum electrodes [36]. The new test cell is capable of 1600 PSI operation in the 5 Tesla LBL Solenoid, recently installed in the MTA, with ionizing radiation from the 400 MeV $H^-$ Linac. IIT, Muons, Inc. and Fermilab staff members prepared a design [37] for a beam line from the Linac to the MTA using available magnets and other components, but the beam line is not expected to be completed until the end of 2008. We had planned to have a demonstration of pressurized high-gradient RF cavities operating in intense magnetic and radiation fields by the end of the STTR Phase II grant period, however the Lab G work was terminated when Fermilab operations removed the klystron from Lab G in January 2004. A klystron became available to us in the MTA in the summer of 2005 without the Solenoid or the implementation of the beam line. The Solenoid began operation in the MTA in March, 2006 and work on high-pressure RF cavities was restarted.

2) **Six-Dimensional (6D) Cooling** using gaseous absorber and pressurized high-gradient RF is the subject of an SBIR grant with Thomas Jefferson National Accelerator Facility (Dr. Yaroslav Derbenev, Subcontract PI), which began in July 2003 and ended in January 2007. A magnetic field configured such that higher energy particles have a longer path length can be used to generate the momentum-dependent energy loss needed for emittance exchange and six-dimensional cooling. In the 6D channel, helical dipole and solenoidal magnets and the RF cavities in them are filled with dense hydrogen so that higher energy particles then have more ionization energy loss. A paper describing the concepts and dynamics of this Helical Cooling Channel (HCC) grew out of the proposal for this grant and has been published in PRSTAB [2]. Recent simulations of a series of four such HCC segments have shown cooling factors of more than 50,000 in a 160 m long linear channel [38]. The 6D grant itself was to support the simulation of the channel by modifying existing computer codes and to optimize the design of the channel.

3) **Hydrogen Cryostat for Muon Beam Cooling** is an SBIR project begun in July 2004 and ended in January 2008 with Fermilab (Dr. Victor Yarba, Subcontract PI) to extend the use of hydrogen in ionization cooling to that of refrigerant in addition to breakdown suppressant and energy absorber. The project is to develop cryostat designs that could be used for muon beam cooling channels where hydrogen would circulate through refrigerators and the beam-cooling channel to simultaneously refrigerate 1) high-temperature-superconductor (HTS) magnet coils, 2) cold copper RF cavities, and 3) the hydrogen that is heated by the muon beam. In an application where a large amount of hydrogen is naturally present because it is the optimum ionization cooling material, it seems reasonable to explore its use with HTS magnets and cold,

but not superconducting, RF cavities. However, the Helical Cooling Channel (HCC) cryostat developed in Phase I, because of new inventions, now has more variants than originally envisioned and there are now several cryostat designs to be optimized. In Phase I we developed computer programs for simulations and analysis and started experimental programs to examine the parameters and technological limitations of the materials and designs of HCC components (magnet conductor, RF cavities, absorber containment windows, heat transport, energy absorber, and refrigerant).

4) **Parametric-resonance Ionization Cooling (PIC)** is a project begun in July 2004 and ended in January 2008 with JLab as a research partner (Dr. Yaroslav Derbenev, Subgrant PI). The excellent 6D cooling expected from the SBIR Project 2 above leaves the beam with a small enough size and sufficient coherence to allow an entirely new way to implement ionization cooling by using a parametric resonance. The idea is to excite a half-integer parametric resonance in a beam line or ring to cause the usual elliptical motion on a phase-space diagram to become hyperbolic, much as is used in half-integer extraction from a synchrotron. This causes the beam to stream outward to large $x'$ and/or $y'$ while the spatial dimensions $x$ and/or $y$ shrink. Ionization cooling is then applied to reduce the $x'$ and $y'$ angular spread. The Phase II grant was to study the details of this new technique and to develop techniques for correction of chromatic and spherical aberrations and other higher-order effects using analytical calculations and numerical simulations.

**5) Reverse Emittance Exchange (REMEX) for Muon Beam Cooling,** with Jefferson Lab (Dr. Yaroslav Derbenev, Subgrant PI) is a Phase I STTR project begun in July 2005 to develop a technique to shrink the transverse dimensions of a muon beam to increase the luminosity of a muon collider. After the 6D cooling described in Project 2 above, the longitudinal emittance is small enough to allow high frequency RF for acceleration. However, the longitudinal emittance after the beam has been accelerated to collider energy is thousands of times smaller than necessary to match the beta function at the collider interaction point. We plan to repartition the emittances to lengthen the muon bunch and shrink the transverse bunch dimensions using linear cooling channel segments and wedge absorbers. A new concept of coalescing bunches to share longitudinal phase space with REMEX was developed in Phase I to enhance collider luminosity.

**6) Muon Capture, Phase Rotation, and Precooling in Pressurized RF Cavities,** with Fermilab (Dr. David Neuffer, Subgrant PI) begun in July 2005 has computational and experimental parts. The use of gas filled RF cavities close to the pion production target for phase rotation and beam cooling will be simulated. In parallel, the project will also involve a continuation of the experimental development in the Fermilab MuCool Test Area (MTA) of high-gradient high-pressure RF cavities operating in a high radiation environment and in strong magnetic fields.

**7) Development and Demonstration of Six-Dimensional Muon Beam Cooling** is with the Fermilab Technical Division (Dr. Rolland Johnson, PI, and Dr. Michael Lamm, subgrant PI). This project is to develop the MANX experiment to prove that effective 6D muon beam cooling can be achieved using an ionization-cooling channel based on a novel configuration of helical and solenoidal magnets. This Helical Cooling Channel (HCC) experiment is being designed with simulations and prototypes to provide an affordable and striking demonstration that 6D

muon beam cooling is understood sufficiently well to become an enabling technology for intense neutrino factories and high-luminosity muon colliders. It is likely that the magnet system developed for this experiment could be used in **9)**, the stopping muon beam proposal now being considered for phase II funding.

**8) Interactive Design and Simulation of Beams in Matter** with IIT (Dr. Thomas J. Roberts, PI, Professor Daniel M. Kaplan, subgrant PI) is to develop G4BeamLine, a beam line design program based on GEANT4 for beams with significant interactions with matter. G4Beamline has been the workhorse for Muons, Inc. and the International Muon Ionization Cooling Experiment (MICE) [39] collaboration to simulate muon cooling channels to explore new techniques. This project is to improve the program for more general use, adding a Graphical User Interface and several new and enhanced capabilities.

**Phase I grants now being proposed for 2008 Phase II projects:**

**9) Stopping Muon Beams** is a project with the Fermilab Accelerator Physics Center, (Dr. Rolland P. Johnson, PI, and Dr. Charles Ankenbrandt, subgrant PI) to develop new techniques to capture and decelerate intense beams of muons for rare decay experiments, muon catalyzed fusion, and muon spin resonance uses. A key ingredient of the plan is to use a helical solenoid magnet as described below for this stopping muon beam application.

**10) Magnets for Helical Cooling Channels** is project to study the technology of the magnets that will be used for helical cooling channels with the Fermilab Technical Division (Dr. Rolland Johnson, PI, and Dr. Alexander Zlobin, subgrant PI).

**11) Compact, Tunable RF** Cavities is a project with the Fermilab Accelerator Division (Dr. Rolland Johnson, PI, and Dr. Milorad Popovic, subgrant PI) to develop new ideas for RF cavities that would be suitable for new applications such as Fixed Field Alternating Gradient Synchrotrons.

Work on these and other projects by Muons, Inc. and collaborators will be presented at EPAC08, where we have submitted 21 abstracts. To see them, go to
http://oraweb.cern.ch/pls/epac08/search.html
Enter the word “muons” in the affiliation field and hit search.

Although each of these projects is independent, taken together they represent a coherent plan to generate a compelling design for an intense muon source. The grants described above support over 14 FTE accelerator scientists. Muons, Inc. now has enthusiastic collaborators from the Illinois Institute of Technology, the Thomas Jefferson National Accelerator Facility, the Fermi National Accelerator Laboratory, Florida State University, the National High Field Magnetic Laboratory, Northern Illinois University, the University of Chicago, and Brookhaven National Laboratory who are part of this effort. This is a creative collaboration dedicated to developing new options for the physics community.

## References

[1] http://www.fnal.gov/projects/muon collider/nu/study/report/machine report/

[2] http://www.cap.bnl.gov/mumu/studyii/FS2-report

[3] http://www.muonsinc.com/mcwfeb07

[4] M. Popovic et al., Linac06

[5] M. Ado, V. I. Balbekov, Sov. At. Energy 31, 731,'71

[6] A. N. Skrinsky and V. V. Parkhomchuk, Sov. J. Part. Nucl. 12, 223 (1981).

[7]D. M. Kaplan, http://www.slac.stanford.edu/ econf/C010630/papers/M102.PDF

[8] P. Gruber, CERN/NUFACT Note 023,
http://slap.web.cern.ch/slap/NuFact/NuFact/nf23.pdf

[9] Bethe, H. A.: Molière's Theory of Multiple Scattering, Phys Rev. **89**, 1256 (1953)

[10] K. Yonehara et al., EPAC06

[11] http://pdg.lbl.gov/2007/reviews/passagerpp.pdf

[12] A. V. Tollestrup & J. Monroe, MUCOOL note 176

[13] W. W. M. Allison et al.,
arxiv.org/PS_cache/physics/pdf/0609/0609195v1.pdf

[14] W. Murray, NuFact05, Frascati

[15] V. Kashikhin et al., Magnets for the MANX Cooling Demonstration Experiment,
MOPAS012, PAC07

[16] S. A. Kahn et al., Magnet Systems for Helical Muon Cooling Channels, MOPAN117,
PAC07

[17] Y. Derbenev and R. P. Johnson, Phys. Rev. Spec. Topics Accel. and Beams 8, 041002 (2005)

[18] R. P. Johnson et al., Linac04

[19] M. BastaniNejad et al.,RF Breakdown in Pressurized RF Cavities, WEPMS071, PAC07

[20] http://wwwasd.web.cern.ch/wwwasd/geant4/geant4

[21] T. J. Roberts et al., G4BL Simulation, PAC07

[22] R. Fernow, ICOOL, http://pubweb.bnl.gov/users/fernow/www/icool/readme.html

[23] M. A. C. Cummings et al., Stopping Muons Beams, THPMN096, PAC07

[24] Yaroslav Derbenev et al., COOL05

[25] D. Newsham et al., Simulations of PIC, PAC07

[26] C. M. Ankenbrandt et al., Muon Bunch Coalescing,, THMN095, PAC07

[27] Meek and Craggs, Electrical Breakdown in Gases, John Wiley & Sons, 1978, p. 557

[28] P. Hanlet et al., EPAC06

[29] D. Neuffer et al., Use of Gas-filled Cavities in Muon Capture, THPMN106, PAC07

[30] E. Barzi, et al. E. Barzi, L. Del Frate, D. Turrioni, R. Johnson, M. Kuchnir (Fermilab & MUONS Inc., Batavia) . 2006. 9pp. Prepared for 2005 Cryogenic Engineering Conference and International Cryogenic Materials Conference (CEC-ICMC 2005), Keystone, Colorado, 29 Aug - 2 Sep 2005. Published in AIP Conf.Proc.824:416-424,2006.

[31] V. Kashikhin et al., PAC07

[32] K. Yonehara et al., Design of the MANX Demon-stration Experiment, PAC07

[33] S. A. Kahn et al., High Field HTS Solenoid for Muon Cooling, MOPAN118, PAC07

[34] Sanborn C. Brown, **Basic Data of Plasma Physics, The Fundamental Data on Electrical Discharges in Gases**, American Vacuum Society Classics, AIP Press, 1993. http://home.earthlink.net/~jimlux/hv/paschen.htm

[35] Y. Derbenev and R. P. Johnson (Phys. Rev. Special Topics Accel. and Beams 8, 041002 (2005)) http://www.muonsinc.com/reports/PRSTAB-HCCtheory.pdf

[36] R. P. Johnson et al., LINAC2004, http://bel.gsi.de/linac2004/PAPERS/TU203.pdf

[37] http://www-mucool.fnal.gov/mcnotes/public/pdf/muc0287/muc0287.pdf

[38] Cool05 http://conferences.fnal.gov/cool05/Presentations/Tuesday/T09_Johnson.pdf

[39] http://hep04.phys.iit.edu/cooldemo/micenotes/public/pdf/MICE0021/MICE0021.pdf

[21] T. J. Roberts et al., G4BL Simulation, PAC07

[22] R. Fernow, ICOOL, http://pubweb.bnl.gov/users/fernow/www/icool/readme.html

[23] M. A. C. Cummings et al., Stopping Muons Beams, THPMN096, PAC07

[24] Yaroslav Derbenev et al., COOL05

[25] D. Newsham et al., Simulations of PIC, PAC07

[26] C. M. Ankenbrandt et al., Muon Bunch Coalescing,, THMN095, PAC07

[27] Meek and Craggs, Electrical Breakdown in Gases, John Wiley & Sons, 1978, p. 557

[28] P. Hanlet et al., EPAC06

[29] D. Neuffer et al., Use of Gas-filled Cavities in Muon Capture, THPMN106, PAC07

[30] E. Barzi, et al. E. Barzi, L. Del Frate, D. Turrioni, R. Johnson, M. Kuchnir (Fermilab & MUONS Inc., Batavia) . 2006. 9pp. Prepared for 2005 Cryogenic Engineering Conference and International Cryogenic Materials Conference (CEC-ICMC 2005), Keystone, Colorado, 29 Aug - 2 Sep 2005. Published in AIP Conf.Proc.824:416-424,2006.

[31] V. Kashikhin et al., PAC07

[32] K. Yonehara et al., Design of the MANX Demon-stration Experiment, PAC07

[33] S. A. Kahn et al., High Field HTS Solenoid for Muon Cooling, MOPAN118, PAC07

[34] Sanborn C. Brown, **Basic Data of Plasma Physics, The Fundamental Data on Electrical Discharges in Gases**, American Vacuum Society Classics, AIP Press, 1993. http://home.earthlink.net/~jimlux/hv/paschen.htm

[35] Y. Derbenev and R. P. Johnson (Phys. Rev. Special Topics Accel. and Beams 8, 041002 (2005)) http://www.muonsinc.com/reports/PRSTAB-HCCtheory.pdf

[36] R. P. Johnson et al., LINAC2004, http://bel.gsi.de/linac2004/PAPERS/TU203.pdf

[37] http://www-mucool.fnal.gov/mcnotes/public/pdf/muc0287/muc0287.pdf

[38] Cool05 http://conferences.fnal.gov/cool05/Presentations/Tuesday/T09_Johnson.pdf

[39] http://hep04.phys.iit.edu/cooldemo/micenotes/public/pdf/MICE0021/MICE0021.pdf

# HIGH TEMPERATURE SUPERCONDUCTORS FOR HIGH FIELD SUPERCONDUCTING MAGNETS

E. Barzi[1], L. Del Frate[1], D. Turrioni[1], R. Johnson[2], and M. Kuchnir[2]

[1]Fermi National Accelerator Laboratory
Batavia, Illinois, 60510, USA

[2]Muons, Inc.
Batavia, Illinois, 60510, USA

## ABSTRACT

Ionization cooling, a method for shrinking the size of a muon beam, requires a low Z energy absorber, high field magnets, and high gradient radio frequency cavities. The use of high temperature superconductors (HTS) for the high field superconducting magnets is being considered to realize a helical muon cooling channel using hydrogen refrigeration. A test stand was set up at Fermilab to perform critical current ($I_c$) measurements of HTS wires under externally applied perpendicular and parallel fields at various temperatures. A description of the test setup and results on $(Bi,Pb)_2Sr_2Ca_2Cu_3O_x$ (BSCCO-2223) tapes and $Bi_2Sr_2CaCu_2O_8$ (BSCCO-2212) round wires are presented. Finally, the engineering critical current density, $J_E$, of HTS and $Nb_3Sn$ were compared in the application's field and temperature range of interest.

**KEYWORDS:** High temperature superconductor, BSCCO, DC measurement.
**PACS:** 74.72.D Hs.

## INTRODUCTION

First generation multi-filamentary HTS are composites of silver or silver alloy matrix and BSCCO. The combination of fine filaments with the metal matrix reduces crack formation and allows critical strain, whether tensile or compressive, in a range of several tenths of a percent [1]. BSCCO conductors are typically produced in the form of tapes and, more recently, of round wires. Tapes are anisotropic and exhibit the highest critical current when the magnetic field is applied parallel to the tape face and the lowest one when the field is perpendicular.

Figure 1 shows the geometrical configuration of a tape and relative directions of magnetic field. The longitudinal direction is along the length of the tape. The transverse direction, orthogonal to the length of the tape, which is parallel to the tape width, is also called "ab-trans" or "lateral" or "long transverse". The transverse direction, orthogonal to the length of the tape, which is perpendicular to the tape face, is also called "c-axis" or "normal" or "short transverse". Magnetic fields having longitudinal or long transverse directions are both parallel to the tape surface. A magnetic field having short transverse direction is perpendicular to the tape surface. In their manufacturing process, the rolling of a wire to tape provides an environment where the superconductor can grow preferentially such that the c-axis of the crystal is mostly perpendicular to the tape face. In the case of the a,b plane there is only a slight difference between the a direction and the b direction (the crystal is nearly tetragonal but slightly orthorhombic) and also there is no preference within the plane of the tape for preferential growth. Because there is little difference in the a and b axis and since there is no preference for growth within the plane, the tape exhibits a nearly isotropic effect in this plane. Critical stresses, determined by the silver alloy sheath, typically range from 50 MPa (for pure silver) up to 130 MPa [2]. For applications where high tensile stresses are encountered, such as high field magnets, stainless steel (SS) reinforcements provide larger stress tolerances. For instance the High Strength BSCCO-2223 tape by American Superconductor (AMSC) withstands up to 265 MPa [1]. Round wires are isotropic, there is no crystallographic texture normal to the wire axis. This is an attractive characteristic because in a magnet configuration the wire will be found in both a perpendicular and a parallel configuration. After reaction the wire is very brittle. High strength tape is commercially available in lengths greater than 100 m, the round wire is available in a range of round sizes and in particular 300 m lengths are available at 0.8 mm diameter.

Results on some earlier BSCCO-2223 and BSCCO-2212 tapes tested at various temperatures can be found in [3]. In [4] critical current and n-value measurements were obtained on BSCCO-2223 tapes, under externally applied perpendicular and parallel magnetic field up to 5 T and temperature between 20 K and 100 K. Results that are available on AMSC web site [5] provide critical currents in a temperature range between 20 K and 77 K and at fields up to 7 T. Dc measurements results on BSCCO-2212 round wire were obtained by Oxford Superconducting Technology (OST) at 4.2 K and at field up to 16 T [6]. For the present application, the choice in temperature ranges from 4.2 K to about 35 K, with the highest possible magnetic field.

## EXPERIMENTAL SETUP

### Samples Description

A High Strength BSCCO-2223 tape, produced by AMSC, and a BSCCO-2212 round wire of 0.8 mm diameter, produced by OST, were tested. Samples specifications are given in Tables 1 and 2 and their cross sections are shown in Figure 2.

### Sample Holders

These HTS critical current measurements were performed at Fermilab at the Short Sample Test Facility. Measurements were obtained at various temperatures in a Variable

Temperature Insert (VTI) with an inner diameter of 49 mm, within a 15/17 T magneto cryostat (Teslatron) by OST.

The minimum critical bending strain for reacted tapes is 50 mm [5]. To avoid sample stress due to bending the tape was tested in the form of straight samples 45 mm long. The wires were provided after reaction in oxygen by OST as straight samples 10 cm long, and they were cut to size. Figure 3 shows the sample holder used to test the BSCCO-2212 wire (left) and the BSCCO-2223 tape (right) in perpendicular and parallel configurations. The tape was tested separately in each configuration. As can be see in Figure (right), for the test in parallel field a force-free configuration was chosen. Sample extremities are soldered directly on the current leads while the central part rests on a G-10 structure. In the design of the sample holders, the length of the soldered junction was chosen [7] to control contact resistance and heating power. The splice length of 12 mm that was used on each side of the sample produced a contact resistance at 4.2 K of ~0.3 μΩ in the case of the tape, most of which due to the SS, and of ~0.1 μΩ in the case of the wire. The current transfer length [8] determined the distance between the voltage taps, which was of 5 mm for the wire, and 10 mm for the tape.

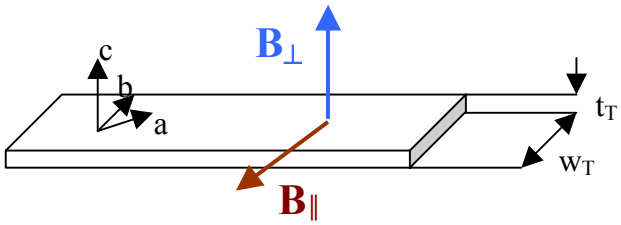


**FIGURE 1.** Geometrical configuration of a BSCCO tape and relative directions of magnetic field.

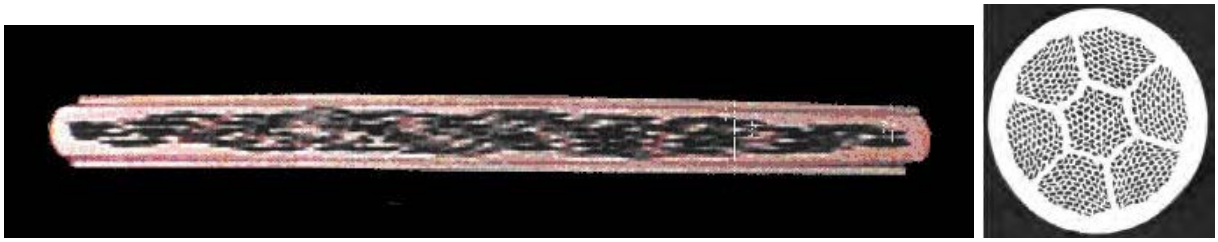

**FIGURE 2.** Transverse cross section of High Strength BSCCO-2223 tape showing 55 filaments of BSCCO-2223 embedded in a metal matrix of silver alloy and 37 μm strips of stainless steel on top and bottom of tape (left). Transverse cross section of unreacted BSCCO-2212 OST 85 × 7 wire (right).

**TABLE 1**. AMSC Tape Specifications

| **High Strength BSCCO-2223 Tape** | |
|---|---|
| Min $I_c$ (77 K, self-field, 1 μV/cm) | 122 A |
| Average thickness | 0.31 mm ± 0.02 mm |
| Average width | 4.16 mm ± 0.02 mm |
| Stainless steel strip thickness | $37 \cdot 10^{-3}$ mm |
| Max. rated tensile strain (95% $I_c$ retention ) | 0.35 % |
| Min. critical bend diameter | 50 mm |

**TABLE 2**. OST Round Wire Specifications

| **BSCCO-2212 Round Wire** | |
|---|---|
| $I_c$ (4.2 K, self-field, 1 μV/cm) | 770 A |
| Average diameter | 0.8 mm |
| Fill factor | 28 % |
| Critical Strain | 0.3 % |

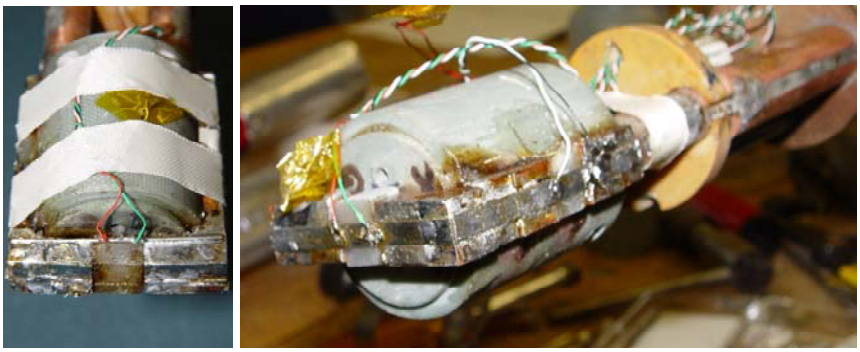

**FIGURE 3**. Sample holder used to test BSCCO-2212 round wire (left), and sample holder used to test BSCCO-2223 tape in perpendicular and parallel configurations (right).

## Measurement Procedure

The current was provided to the sample using 1000 A current leads. Voltage-current (VI) characteristics were measured in He (liquid or vapor) at a magnetic field up to 15 T. The $I_c$ was determined from the VI curve using the 1 μV/cm criterion. The n-values were determined in the $V(I_c)$ to $10 \cdot V(I_c)$ range by fitting the VI curve with the power law $V \sim I^n$. In the case of the tape, critical current measurements were also performed at zero magnetic field in liquid nitrogen at 77 K.

Table 3 shows the results of the $I_c$ measurement error analysis at 4 T. The effects that were considered include temperature variations, magnetic field variations (only for vertical samples, as for the horizontal ones this effect is negligible), self-field, noise. The read-back accuracy of the power supply is 0.1 % + 0.6 A. In addition, an accuracy of 1 mm in placing voltage taps leads to $\Delta I_c/I_c =$ 0.6 to 10 % for n-values ranging from 34 to 2.

**TABLE 3**. Results at 4 T of $I_c$ measurement error analysis

| $\Delta I_c / I_c$ | At 4.2 K | At 14 K | At 22 K | At 38 K |
|---|---|---|---|---|
| Due to ΔT @ 4 T | - 0.14 % | -0.15 % | - 0.26 % | - 1.66 % |
| Due to ΔB @ 4 T for vertical samples | - 0.06 % | - 0.07 % | - 0.08 % | - 0.1 % |
| Self-field effect @ 4 T | 0.6 % | 0.7 % | 0.8 % | 0.9 % |
| Noise effect @ 4 T | 0.17 % | 0.28 % | 0.69 % | 0.22 % |

## RESULTS AND DISCUSSION

### BSCCO-2223 Tape

Figures 4 and 5 show $I_c$ results as a function of magnetic field for the BSCCO-2223 tape, in the parallel and perpendicular field configuration respectively, tested from 4.2 K up to 34 K. The $I_c$ test results in nitrogen at 77 K were of 125 A for the tape tested in parallel configuration and of 127 A for the tape tested in perpendicular configuration.

Figures 6 and 7 show $I_c$ results as a function of temperature at various fields, in the parallel and perpendicular field configuration respectively.

Figure 8 shows n-value results as function of applied field at various temperatures in the perpendicular configuration.

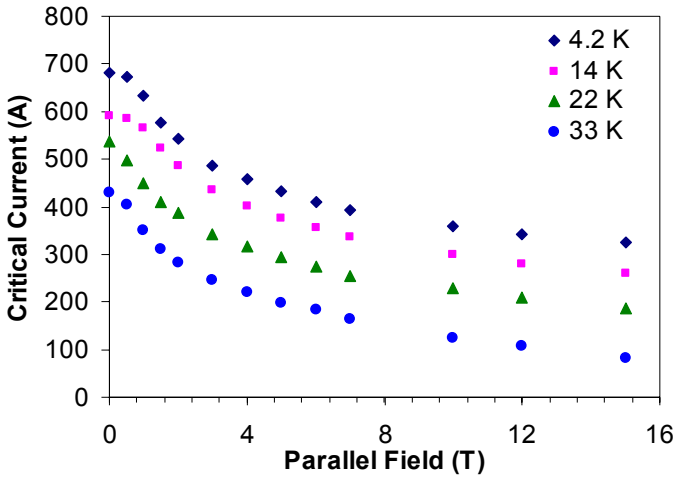


**FIGURE 4**. AMSC BSCCO-2223 High Strength tape $I_c$ results as a function of applied magnetic field at various temperatures in parallel configuration.

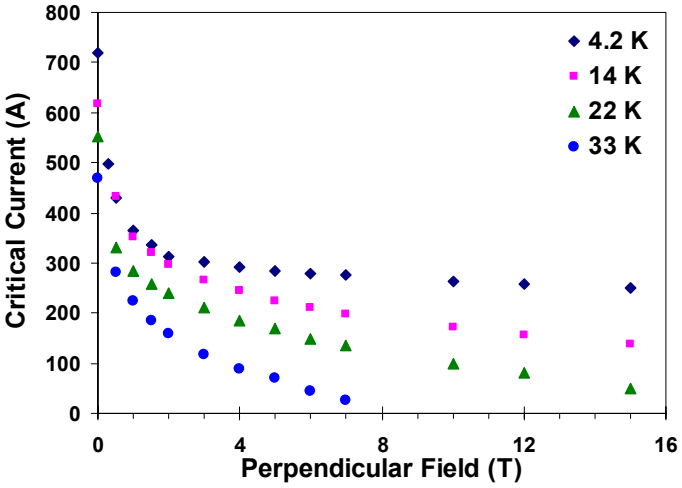


**FIGURE 5.** AMSC BSCCO-2223 High Strength tape $I_c$ results as a function of applied magnetic field at various temperatures in perpendicular configuration.

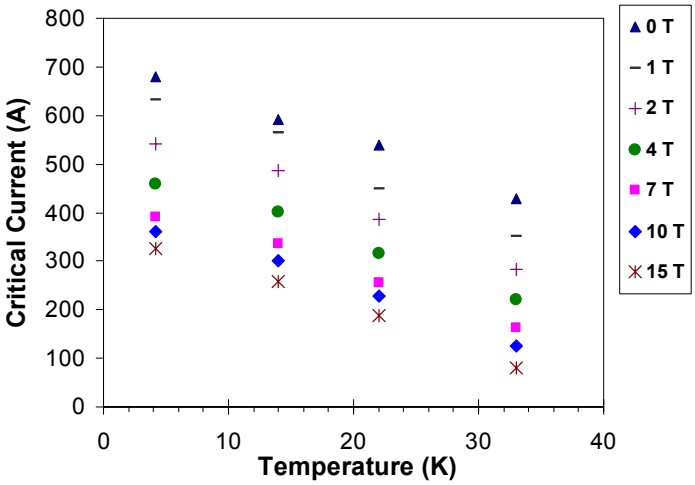


**FIGURE 6**. AMSC BSCCO-2223 High Strength tape $I_c$ results as a function of temperature at various applied magnetic fields in parallel configuration.

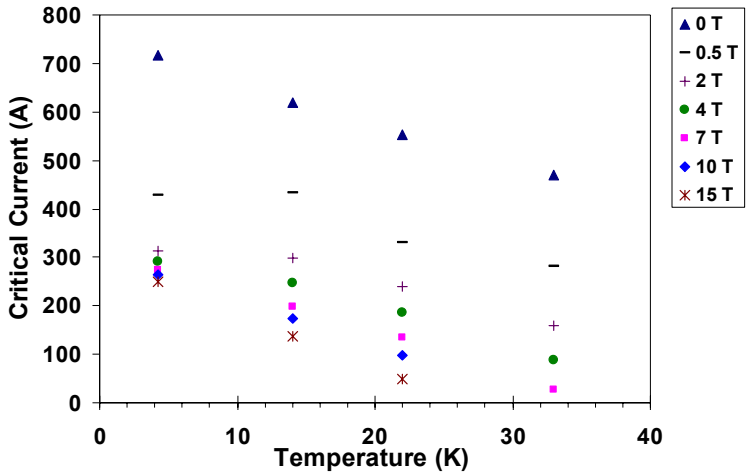


**FIGURE 7**. AMSC BSCCO-2223 High Strength tape $I_c$ results as a function of temperature at various applied magnetic fields in perpendicular configuration.

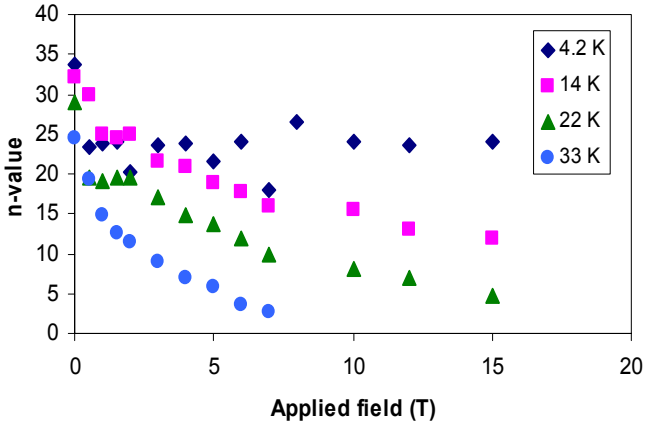


**FIGURE 8.** AMSC BSCCO-2223 High Strength tape n-value results as a function of applied magnetic field at various temperatures in perpendicular configuration.

## BSCCO-2212 Round Wire

Figure 9 shows $I_c$ results as a function of magnetic field for the BSCCO-2212 round wire, tested from 4.2 K up to 34 K. Figure 10 shows $I_c$ results as a function of temperature at various fields. Figure 11 shows n-value results as a function of applied field at various temperatures.

Figure 12 shows the $J_E$ results obtained at 4.2 K for three different samples and the value obtained by the company [6]. These data provide a measure of reproducibility when testing identical samples, and of consistency with the company's results.

## Comparison with LTS

Figures 13 and 14 show a comparison between HTS, $Nb_3Sn$ and NbTi performance in form of $J_E$ as a function of field at 4.2 K and 14 K respectively. The wire shows lower critical current but higher $J_E$ than tapes, also because of the stainless steel strips reducing the transport current area. At 4.2 K $Nb_3Sn$ performs better at least up to magnetic fields of 17 T, while the superiority of the HTS materials is obvious at higher temperatures.

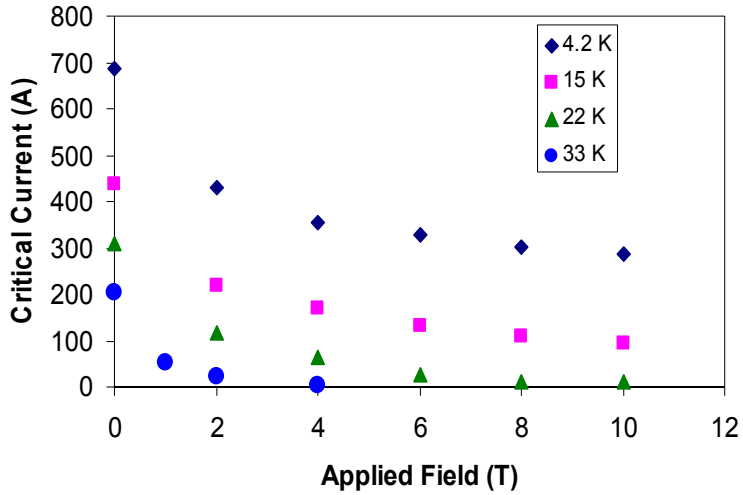


**FIGURE 9**. OST BSCCO-2212 round wire $I_c$ results as a function of applied field at various temperatures.

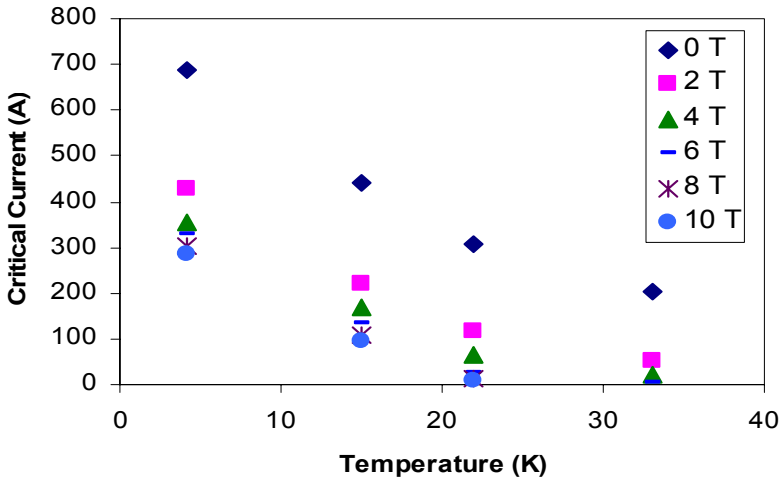


**FIGURE 10**. OST BSCCO-2212 round wire $I_c$ results as a function of temperature at various applied fields.

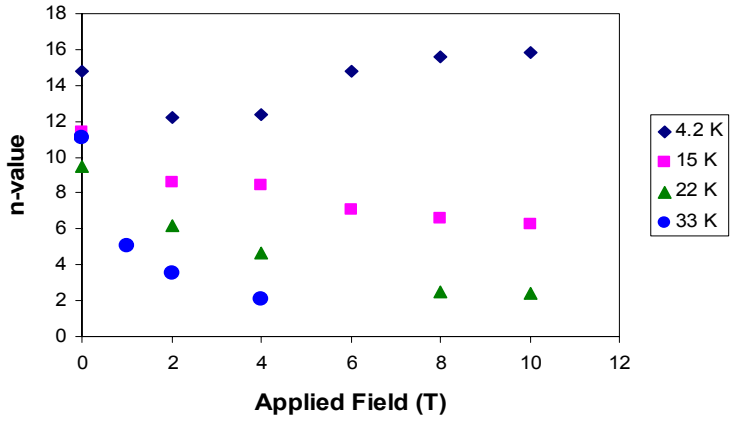


**FIGURE 11.** OST BSCCO-2212 round wire n-value results as a function of applied field at various temperatures.

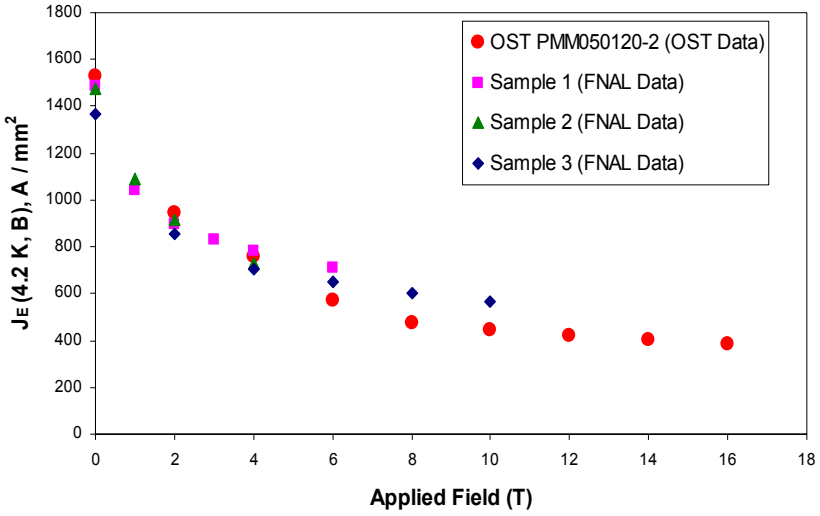


**FIGURE 12.** OST BSCCO-2212 round wire $J_E$ results as a function of applied field at 4.2 K for three different samples and comparison with company's data.

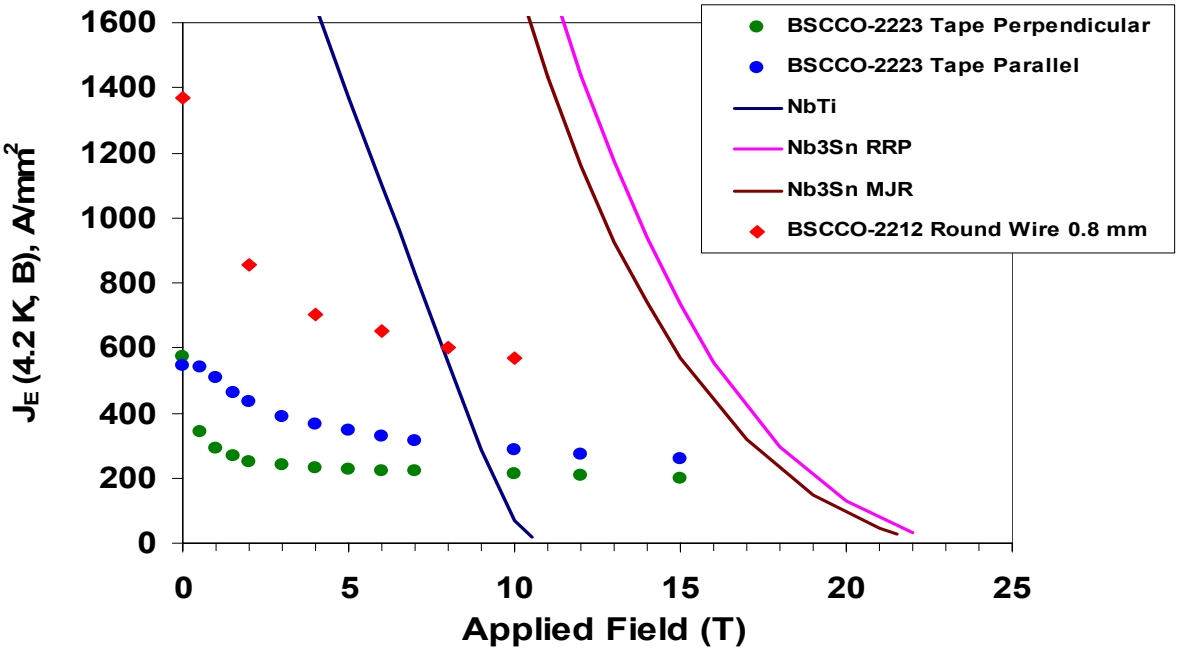


**FIGURE 13.** $J_E$ comparison at 4.2 K between NbTi, $Nb_3Sn$, BSCCO-2212 wire and BSCCO-2223 tape as a function of applied magnetic field.

## CONCLUSIONS

A measurement apparatus was set up to measure the dc characteristics of HTS tapes and wires under applied magnetic fields at various temperatures. Test temperatures from 4.2 K to 34 K were achieved for BSCCO-2223 tapes and a BSCCO-2212 round wire while providing up to 1000 A of current and magnetic field magnitudes up to 15 T. The data acquired from the measurements performed using the designed sample holders are consistent with similar

measurements performed by AMSC [5] and OST [6]. A comparison between HTS, $Nb_3Sn$ and NbTi was obtained in the range of temperature and field of interest to help choose the most adequate superconductor for the magnets of a muon cooling channel application.

Studies of strain effects on the superconducting properties will also be performed to determine whether a React&Wind or Wind&React technology should be used. Once the operation temperature and magnetic field operation range of the magnets will have been specified, magnetization measurements might also be of interest.

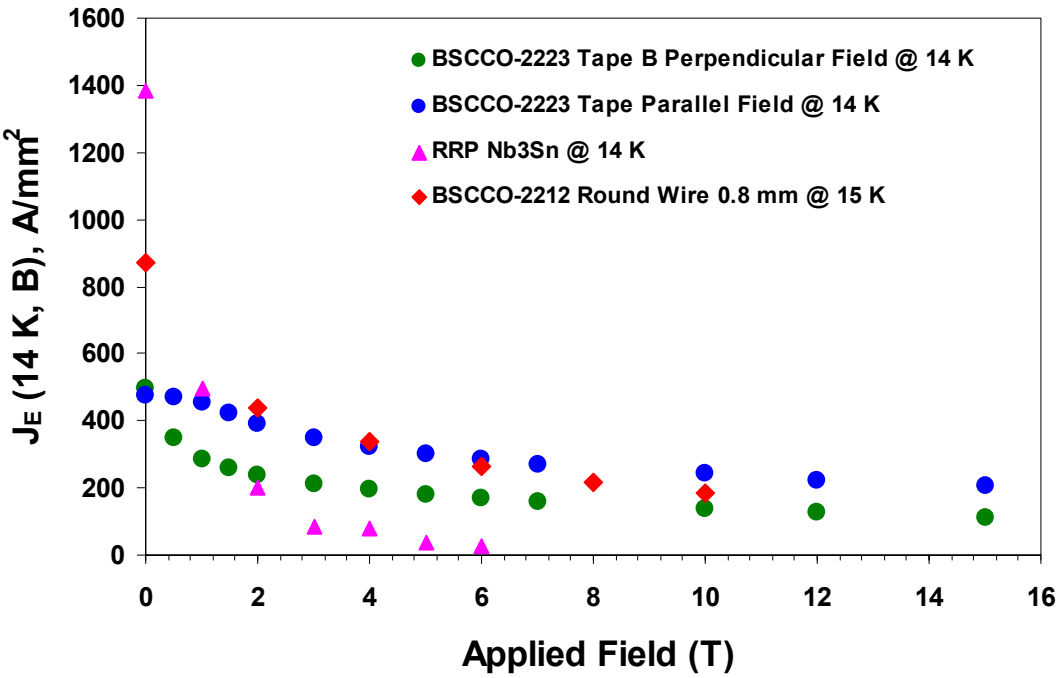


**FIGURE 14.** $J_E$ comparison at 14 -15 K between $Nb_3Sn$, BSCCO-2212 wire and BSCCO-2223 tape as a function of applied magnetic field.

## ACKNOWLEDGMENTS

The authors express their appreciation to Ado Umezawa at AMSC and Ken Marken at OST, Inc., for providing the HTS superconducting samples. This work is supported by DOE STTR grant DE-FG02-04ER86191 # rol@muonsinc.com.

## REFERENCES

1. Masur L. J. et al., IEEE Trans. Appl. Sup., V. 11 (2001), p. 3256.
2. Fischer K. et al., IEEE Trans. Appl. Sup., V. 9 (1999), p. 2625.
3. L. F. Goodrich and T. C. Stauffer, “Hysteresis in transport critical current measurements of oxide superconductors”, NIST J. Res., V. 106, p. 657, 2001.
4. M. A. Young et al., IEEE Trans. Appl. Sup., V. 13, No. 2, June 2003, p. 2964.
5. Information available at http://www.amsuper.com/products/htsWire/103419093341.cfm.
6. H. Miao, K. R. Marken, M. Meinesz, B. Czabaj and S. Hong, IEEE Trans. Appl. Sup., V. 15 (2005), p. 2554.
7. Wilson N. M., “Superconducting magnets”, Clarendon Press, Oxford.
8. Ekin J. W., Appl. Phys. , 49 (1978), p. 3406.

# Superconducting Helical Solenoid Systems for Muon Cooling Experiment at Fermilab

Vladimir S. Kashikhin, Nikolai Andreev, Rolland P. Johnson, Vadim V. Kashikhin, Michael J. Lamm, Gennady Romanov, Katsuya Yonehara, Alexander V. Zlobin

***Abstract*— Novel configurations of superconducting magnet system for Muon Beam Cooling Experiment is under design at Fermilab. The magnet system has to generate longitudinal and transverse dipole and quadrupole helical magnetic fields providing a muon beam motion along helical orbit. It was found that such complicated field configuration can be formed by a set of circular coils shifted in transverse directions in such a way that their centers lay on the center of the helical beam orbit. Closed beam orbit configurations were also proposed and investigated. This paper describes the magnetic and mechanical designs and parameters of such magnetic system based on a NbTi Rutherford type cable. The helical solenoid fabrication, assembly and quench protection issues are presented.**

***Index Terms*—Helical Solenoid, Magnetic Design, Muon Cooling, Superconducting Magnet System.**

## I. INTRODUCTION

THE 6-dimensional muon ionization-cooling experiment is now under design at Fermilab [1-2]. The main magnet system of this experiment is a Helical Cooling Channel (HCC). Two superconducting concepts of HCC were investigated. The first has a large bore (~ 1 m diameter) superconducting solenoid with outer helical dipole and quadrupole coils. The second is a helical superconducting solenoid of 0.5 m diameter with the coil sections shifted in the transverse direction to simultaneously generate solenoidal, helical dipole and helical quadrupole field components. Both magnet system concepts were discussed in [3]. The comparison showed the advantage of the Helical Solenoid (HS) from a magnet system point of view. The HS has half the coil diameter and superconductor volume, seven times lower total magnetic field energy, lower peak field in the superconductor (5.7 T vs. 7.6 T), a correspondingly lower level of Lorentz forces and naturally generated helical dipole and quadrupole fields. This more efficient concept of HS was chosen for further investigation and briefly discussed in [4,5]. This paper summarizes further investigations of the HCC for muon beam cooling. Proposed novel beam closed orbit magnet system configurations.

Manuscript received August 27, 2007. This work was supported in part by the U.S. Department of Energy under STTR Grant DE-FG02-04ER86191 and -06ER86282..

V. S. Kashikhin, N. Andreev, V. V. Kashikhin, M. J. Lamm, K. Yonehara, A. V. Zlobin are with the Fermi National Accelerator Laboratory, Batavia, IL 60510 USA (corresponding author phone: 630-840-2899; fax: 630-840-3369; e-mail: kash@fnal.gov).

R. P. Johnson is with Muons Inc., Batavia, IL 60510 USA.

## II. SINGLE HELICAL SOLENOID

The Single Helical Solenoid (SHS) described in [3] has the general parameters and geometry shown in Fig. 1 and Table I.

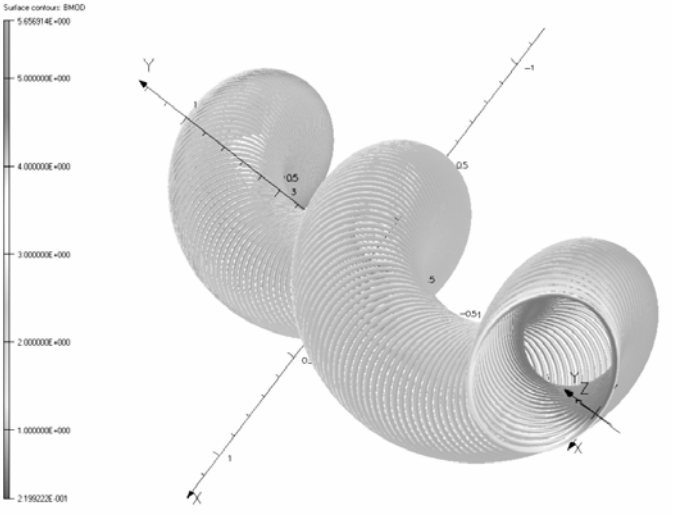

Fig. 1. Helical Solenoid geometry and flux density.

TABLE 1 Helical Solenoid Parameters

| Parameter | Unit | Value |
|---|---|---|
| Inner bore diameter | m | 0.5 |
| Helical Solenoid length | m | 4.0 |
| Helix twist pitch | m | 1.6 |
| Radius of beam reference orbit | m | 0.255 |
| Initial dipole field, $B_\tau$ | T | 1.25 |
| Dipole field gradient, $\partial B_\tau/\partial z$ | T/m | -0.17 |
| Initial quadrupole field, $\partial B_\tau/\partial r$ | T/m | -0.88 |
| Quadrupole field gradient, $\partial^2 B_\tau/\partial r/\partial z$ | $T/m^2$ | 0.07 |
| Initial field, $B_z$ | T | -3.86 |
| Longitudinal field gradient, $\partial B_z/\partial z$ | T/m | 0.54 |
| NbTi superconductor peak field | T | 5.7 |
| Operational current | kA | 10 |
| Operating stored energy | MJ | 4.4 |
| Coil section length along Z axis | mm | 20 |
| Superconducting cable length | km | 3.3 |

The main concept of this approach is to use circular short coils shifted in the transverse direction to the z axis. All coil centers lay on a helical beam orbit and are equally distributed along z. Because each coil is tilted relative to the helical beam

orbit direction, it simultaneously generates longitudinal and transverse field components. The inner volume of the magnet system is filled with a liquid helium (LHe) or a hydrogen gas which are energy absorbers for the ionization-cooling experiment.

The muon momentum is reduced from 300 MeV/c to 160 MeV/c in passing along the 5.6 m helical path through the LHe absorber. and the magnetic field strength must diminish with the momentum to provide a stable beam orbit. Magnetic field simulations were performed to investigate the behavior of the SHS. Fig. 2 shows the relative field components for a model in which the current in the coils was decreased linearly as a function of the longitudinal z-coordinate with gradient -13 %/m.

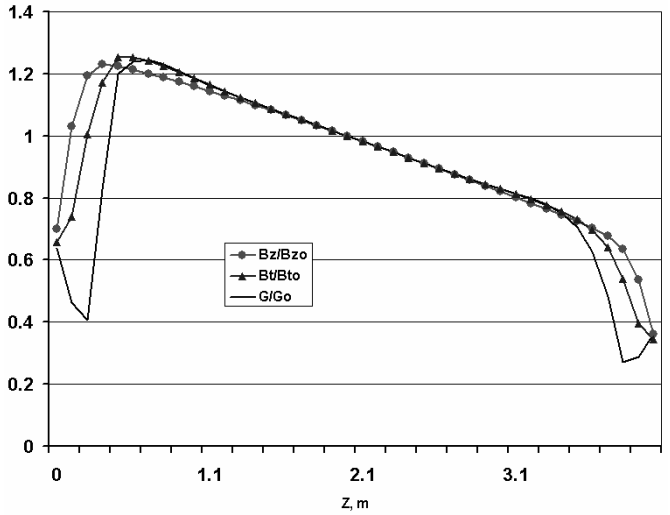


Fig. 2. Field distribution related to the values at z=2 m (Bzo=-3.37 T, Bto=1.04 T, Go=-0.9 T/m).

One can see the interesting result that the three important field components, (solenoidal (Bz), helical dipole (Bt), and helical quadrupole (Gz)), scale with the coil currents. Fig. 3 shows the dependence of the three field components as a function of coil radius.

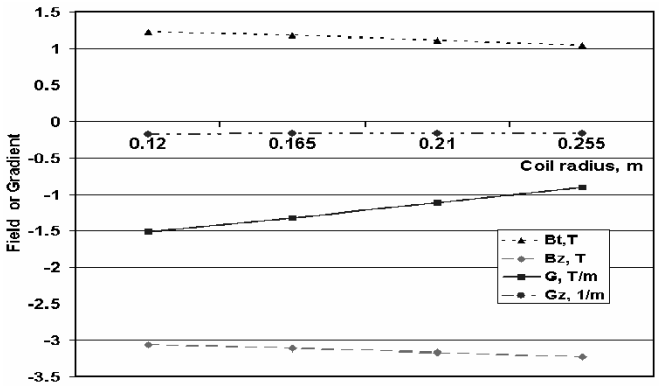


Fig. 3. Field and field gradient dependence.

As follows from Fig. 3 there is a linear dependence of field components and gradient with the coil radius change. At the same time Gz gradient is constant and defined only by coil currents.

The Helical Solenoid have fixed helical dipole and quadrupole fields. The muon cooling experiment will be more attractive if helical dipole and quadrupole fields will be regulated in wide range of helical field levels independently from the Bz solenoidal field. The helical dipole and quadrupole coils should correct ~30 % of corresponding field component.

## III. Double Helical Solenoid

The Single Helical Solenoid will occupy only a spiral space inside cylindrical ~1 meter diameter liquid helium vessel. There is enough space to place the second Helical Solenoid shifted on a half helix twist pitch in longitudinal direction. Fig. 4 shows the Double Helical Solenoid (DHS) of novel configuration. The direction of currents in opposite sections defines if the longitudinal Bz field components have the same or opposite directions. The same Bz field directions for the DHS channels open a possibility to use this system for particles having the same sign of charge. Another more attractive opportunity is to have opposite currents and Bz fields (see Fig. 5) in opposite coils. So, positive and negative muons could be cooled in parallel channels. In this case also both helical channels could be used in a closed orbit configuration. The DHS parameters for this option are shown in Table 2. One can see that in DHS with opposite currents the transverse Lorentz forces goes to the system center and self-compensated. It reduces demands to the outer mechanical support structure and provides better mechanical stability of superconducting coils.

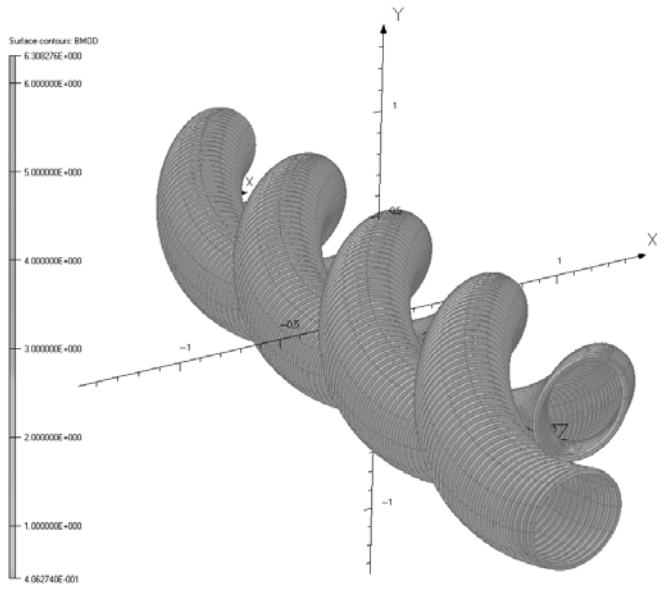


Fig. 4. Double Helical Solenoid geometry and flux density.

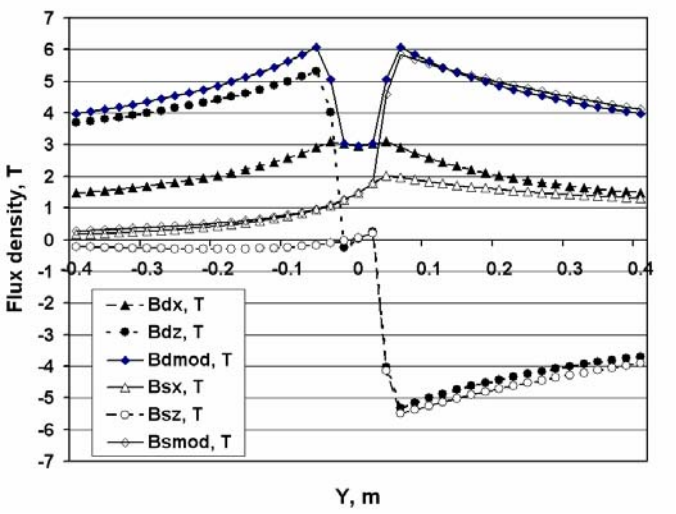


Fig. 5. Field distribution in 3.2 m Single and Double Helical Solenoids at z=1.6 m and x=0. Field components Bsx, Bsz, Bsmod are for single and Bdx, Bdz, Bdmod are for double solenoid.

TABLE II Double Helical Solenoid Parameters

| Parameter | Unit | Value |
|---|---|---|
| Inner coil diameter | m | 0.42 |
| Double Helical Solenoid length | m | 1.6 |
| Helix twist pitch | m | 1.6 |
| Radius of beam reference orbit | m | 0.255 |
| NbTi superconductor peak field | T | 6.3 |
| Operational current | kA | 10 |
| Operating stored energy | MJ | 4 |
| Coil section length along Z axis | mm | 20 |
| Superconducting cable length | km | 2.2 |

As follows from Fig. 5 the Bz field components are close for SHS and DHS. The transverse Bx field components in beam area are in range of 1.5 – 2 Tesla but DHS has two times larger $\partial B_r/\partial r$ transverse gradient -3.3 T/m and -1.65 T/m correspondingly. In [3] was shown the linear dependence between SHS optimal transverse gradient for a longitudinal cooling and the helix period. For SHS with 0.5 m coils inner diameter the optimal helix period is 1.6 m. For DHS with 0.42 m coil diameter and larger gradient the helix period should be reduced and optimized.

## IV. Closed Orbit Magnet Systems

The proposed SHS and DHS muon cooling channels could be used for muon beam cooling in closed orbit configurations. The main advantage of closed orbit systems are to extremely reduce the total future channel cost, incorporate room temperature [6-10] or even superconducting RF cavity to compensate muon energy losses in absorber, and improve the total cooling channel performance using multi turn beam circulation. Fig. 6 shows the view of muon cooling experiment based on SHS.

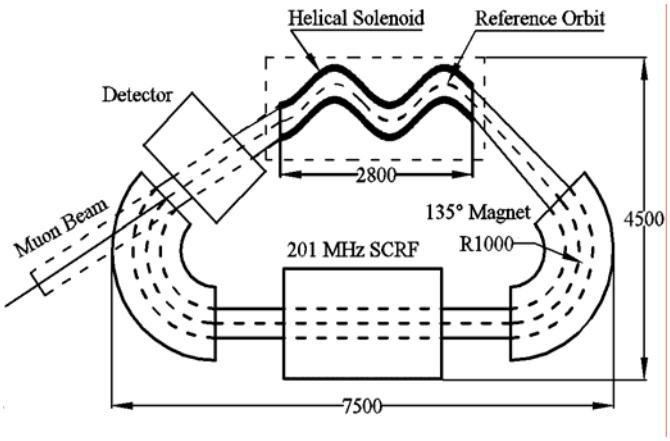


Fig. 6. Schematic view of muon cooling experiment with Single Helical Solenoid. All dimensions in mm.

The system includes: SHS, three combined function magnets which provide beam closed and stable orbit, 201 MHz superconducting or room temperature RF cavity, and muon detector. All magnets and SCRF could have common cryostat and beam pipe. The 320 mm diameter beam pipe could be filled with hydrogen gas used as an absorber. The beryllium foils and wedges used as gas absorber breakers and additional absorbers. The combined function magnets should have ~ 1.1 T dipole magnetic field, plus quadrupole and sextupoles correctors. The SCRF cavity is shielded from external magnetic fields by an iron shield to the level of several μT. During experiments to obtain optimal cooling the absorber gas pressure is regulated to match the RF cavity integrated gradient and the absorber energy losses. The helical solenod has helical dipole and quadrupole correctors to optimize the ionization cooling and provide stable closed orbit. Because muons have a very short life time (~ 5.6 μs at energy 250 MeV/c ) the number of turns and particle path length is limited. More compact magnet system could be built on the base of DHS. Fig. 7 shows the view of such system where at the end of the cooling channel the muon beam rotated by 270° and goes in opposite direction through the second helical solenoid in the DHS.

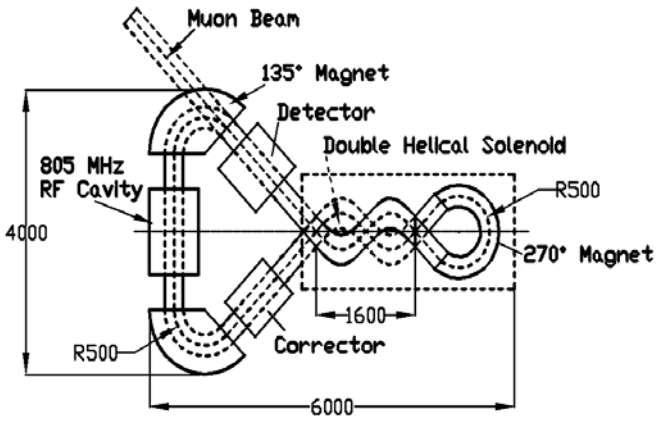


Fig. 7. Schematic view of muon cooling experiment with Double Helical Solenoid. All dimensions in mm.

The closed orbit beam circulation where beam goes in opposite directions in helical channels and turned back at the cooling channel ends by dipole magnets has more compact configuration and better combined with 805 MHz cavity [9]. All magnets have main dipole coils, quadrupole and sextupole correctors. Besides the multipole corrector placed at the exit from the Helical Channel to focus the beam for further transportation. The goal of this section is to propose for investigation closed orbit configurations. The obvious difficulties are: the beam injection and proper matching with the Helical Channel, beam transportation without emittance grouth and losses, correct synchronization RF cavity phase and beam. But all of these overcompensated by substantial cost reduction of cooling channel for future muon accelerators and the experimental possibility to confirm the ionization cooling effect for the muon beam.

## V. Short Model Prototype

The Helical Solenoid generates complicated helical field components and corresponding Lorentz forces. These forces are intercepted by the outer collar structure. Fig. 8 shows a mechanical design of a short (~100 mm long) solenoid section to be used as a prototype to prove the SHS design and manufacturing technology.

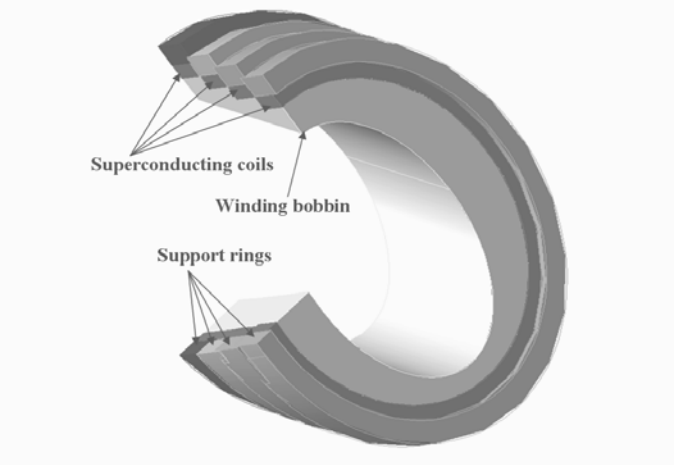


Fig. 8 Helical Solenoid short section geometry.

Single layer coils are continuously hard bend wound with NbTi Rutherford type SSC cable on an inner support cylinder, while outer collar rings are correspondingly mounted, section by section. After assembly, rings are welded to each other, the whole assembly is vacuum impregnated with epoxy, forming a solid mechanical structure. Mechanical stresses at a nominal current in this cold mass assembly are less than 50 MPa. The level of stresses well models the long Helical Solenoid mechanical structure. For the long solenoid a one meter diameter outer stainless steel tube will be used as the solenoid support structure and as an outer wall of liquid helium vessel. This tube will protect the magnet system from longitudinal and transverse motion under Lorentz forces.

## VI. Conclusion

The proposed magnet system configurations are very promising for further investigations. The careful beam optics analysis with control of total muon cooling effect should be made to confirm the efficiency of closed orbit magnet systems. Also should be designed beams injection, extraction and detection systems for which could be used conventional particle accelerator technology.

Nevertheless, it is possible to highlight the following advantages:

- Single Helical Solenoid provides effective 6-D muon beam ionization cooling (see [4] and [5]);
- Double Helical Solenoid could be used for ionization cooling of two muon beams with opposite particle charge;
- Single and Double Helical Solenoids provide effective way of building the closed orbit cooling channels with open for RF cavity installation structure.
- Dipole magnets at the ends of magnet system combined with gas absorbers or beryllium wedges in addition capable to increase beam cooling efficiency;
- It is convenient at closed orbit system ends inject and extract the beam;
- RF could be mount in a very low magnetic field region and even superconducting RF technology could be used;
- An absorber gas pressure inside the helical channel could be regulated to match RF structure integrated acceleration gradient;
- Closed orbit system configurations extremely reduce the cooling channel cost and improve muon beam cooling efficiency by multi turn passing.

## References

[1] Y. Derbenev, R.P. Johnson, Phys. Rev. STAB 8, 041002, 2005.
[2] R. Gupta et al., “Letter of intent to propose a six-dimensional muon beam cooling experiment for Fermilab” http://www.muonsinc.com/tiki_download_wiki_attachment.php?attId=36
[3] V.S. Kashikhin, *et al.*, “Superconducting magnet system for muon beam cooling”, Proceedings of Applied Superconductivity Conference, ASC 2006.
[4] V. S. Kashikhin, *et. al.*, “Magnets for the MANX 6-D cooling demonstration experiment”, Particle Accelerator Conference, Albuquerque, 2007, to be published.
[5] K. Yonehara *et al.*, "The MANX muon cooling demonstration experiment", Particle Accelerator Conference, Albuquerque, 2007, to be published.
[6] A. Moretti, *et. al.*, “RF cavities for the muon and Neutrino Factory collaboration study”, XX International Linac Conference, Monterey, California.
[7] J. Corlett *et al.*, ”High-Gradient normal-conducting RF structures for muon cooling channels” PAC2001, Chicago, 2001
[8] J. Corlett *et al.*, “RF accelerating structures for the muon cooling experiment “, PAC’99, New York, March 29-April2, 1999.
[9] Derun Li *et al.,* “Design and fabrication of an 805 MHz RF cavity with Be windows for a high RF power testing for a muon cooling experiment”, PAC2001, Chicago.
[10] A. Moretti, *et al.*, “π/2 interleaved cavity developments for the muon collider cooling experiment”, Linear Accelerator Conference, Chicago 1998.

# Optimization of Brittle Superconducting $Nb_3Sn$ Strand Designs

M. Alsharo'a, E. Barzi, M. Bossert, R. P. Johnson, D. Turrioni, R. Yamada, A. V. Zlobin

*Abstract*—**Finite element simulations and experimental measurements of $Nb_3Sn$ deformed strand cross sections were performed to study their structural behavior during cabling. A variety of $Nb_3Sn$ strand designs were modeled to identify and optimize design parameters like sub-element shape, number of sub-elements, and their spacing. The model results were correlated to the experimental results. This led to a numerical-experimental approach that is effective in predicting fracture, merging, and deformation of the sub-elements. Strains were calculated as a function of strand deformation for strands with 54, 120, and 210 sub-elements and a local Cu-to-non-Cu ratio of 0.165. Strains as a function of strand deformation were also calculated for 120/127 strands with a local Cu-to-non-Cu ratio of 0.11, 50% increased spacing, and 100% increased spacing between sub-elements. Results showed that increasing the spacing by 100% reduces the maximum strain-x, maximum strain-y, and maximum strain-xy by 14%, 13%, and 29% respectively at a 30% strand deformation level. Also, results revealed that the maximum strain components are always located in the sub-elements close to the center of the strands, which agrees with the experimental findings.**

*Index Terms*—**$Nb_3Sn$ plastic deformation, $Nb_3Sn$ strain, $Nb_3Sn$ strands, Restacked Rod Process.**

## I. Introduction

THE Restack Rod Process (RRP) is the $Nb_3Sn$ strand technology presently producing the largest critical current densities at 12 T and 4.2 K. Due to the plastic deformation that occurs during cabling, which is one of the main factors of strand current degradation at both high and low fields [1], sub-elements (SE) may merge into each other, creating larger filaments with a continuous barrier. In this case, the strand recognizes a larger effective filament size and its instability can considerably increase locally, leading to cable quench [1].

Finite element studies performed for $Nb_3Sn$ wires to be used for The Next European Dipole (NED) activity showed that finite element analysis is a powerful tool to simulate severe plastic deformations of $Nb_3Sn$ strands before the rupture of the sub-elements [2]. In this paper, the deformation resulting from the cabling process was simulated and compared to experimental results. Plastic deformation was studied numerically for a variety of cases. Comparing the numerical results with the experimental data yields the strain values corresponding to fracture in the sub-element. The advantage of this numerical approach is its ability to anticipate failure without the need to perform detailed deformation experiments.

To reduce the merging effect of the sub-elements, Oxford Instruments Superconducting Technology (OST) developed a new RRP strand design with a 50% increase in Cu spacing between the sub-elements arranged in a 60/61 array (RRP2). A comparison study was performed between a regular strand with 54/61 array (RRP3) [3] and the spaced design (RRP2) using 0.7 mm round strands. Damage analysis comparisons showed that sub-element breakage is similar, but their merging behavior is different. The RRP2 design was proven to be effective in reducing merging [1], [4].

In this work, RRP3 and RRP2 strands were modeled and compared with the experimental measurements. To study the effect of the number of sub-elements on the deformation, strands with 54/61, 120/127, and 210/217 arrays were modeled up to 30% deformation level. All had the same Cu spacing (local Cu-to-non-Cu ratio of 0.165) between sub-elements. To study the effect of the Cu spacing between the sub-elements on the deformation, the 120/127 strand was modeled for three cases: regular spacing (local Cu-to-non-Cu ratio of 0.11), 50% increased spacing, and 100% increased spacing. To provide experimental data, strands were rolled down to decreasing thicknesses to cover a range of deformations up to 35%. Cross sections of rolled strands were then studied using microscopy analysis where the longest and shortest sizes of each sub-element were measured using a high resolution optical microscope equipped with imaging software.

## II. Finite Element Modeling

The round composite strand, with niobium and tin sub-elements, embedded in a Cu matrix, was modeled. In order to make the modeling closer to reality, at first the exact geometry of the sub-elements, obtained using microscopy pictures of the strand cross sections, was implemented in the finite element model. Hexagonal sub-elements were eventually used (see next Section). To reduce the model complexity, a two-dimensional model with perfect bonding between Cu, niobium, and tin was considered. To take advantage of the symmetry, only one quarter of the full geometry was modeled. Contact analysis was performed to model the severe compression process using ANSYS [5]. Rigid contact surfaces were created on both sides of the strand as shown in Fig. 1. Two-dimensional, 8-node, plane elements with large strain

Manuscript received August 28, 2007. This work was supported in part by the U.S. Department of Energy under Grants DE-FG02-04ER86191, DE-FG02-07ER84825, and DE-AC02-07CH11359 (Sponsor is Muons, Inc. Batavia IL. Web: www.muonsinc.com).

M. Alsharo'a (corresponding author, phone: 630-857-8881; e-mail: sharo@muonsinc.com), and R. P. Johnson are with Muons, Inc. Batavia, IL, 60510, USA.

E. Barzi, M. Bossert, D. Turrioni, R. Yamada, and A. V. Zlobin are with Fermi National Accelerator Laboratory, Batavia, IL, 60510, USA.

capability were used. Compression loads, vertical to the contact surfaces, were then applied to compress the strands. Direction of loading was predicted from the direction of deformation revealed in the microscopy pictures (usually in the y-direction perpendicular to the contact surfaces). Material properties over both the elastic and plastic strain ranges were included in the model to model the plastic deformation [6]. The choice of the correct stress-strain curves was critical in improving the accuracy of the results.

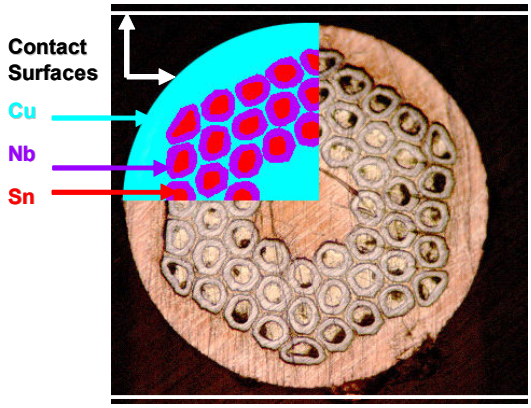


Fig. 1. The actual geometry of the RRP3 strand and the finite element model. The figure shows the components of the strand and the contact surfaces.

## III. Verification of the Finite Element Modeling

The 60/61 array (RRP2) strand, with an original diameter of 0.7 mm, was subjected to rolling loads and compressed to depths of 0.55, 0.5, and 0.45 mm. A corresponding finite element model was built and validated through comparisons of the finite element deformed strand shapes with a number of microscopy pictures of strand cross sections at each deformation stage. Fig. 2 shows the actual and finite element geometries of the RRP2 strand. Figs. 3, 4, and 5 show comparisons of the simulated deformed geometries with the experimental images at various deformation levels. From these and a number of other strand cross sections, it was observed that breakage starts in the inner elements. Some breakage in the outer elements also occurs in correspondence of the 45° planes. At the largest deformations, breakage spreads out from the center along the 45° planes.

In addition to the comparisons of the finite element deformed shapes of RRP2 to the corresponding experimental images, the model was also compared quantitatively to the experimental measurements. The average of both the longest and shortest sizes of all the sub-elements in the cross section were measured and compared to the corresponding numerical calculations at various deformation levels as shown in Fig. 6. Error bars represent the standard deviation of the distributions and are a measure of the size spread between sub-elements. In Fig. 6, numerical results are shown for both the model that used hexagonal sub-elements and the model that used sub-elements with their actual shapes. As can be seen, the hexagonal model slightly underestimates the sub-element sizes, but the model with actual shapes of the sub-elements produces a better prediction of the shortest sub-element size. Either model doesn't simulate fracture or merging of sub-elements. Consequently, the spread in their sizes is not accurately represented. Due to the fact that the differences between the two models are minor, the hexagonal model was eventually adopted. Figs. 7, 8, and 9 show the strain results for the case of 0.45 mm final depth.

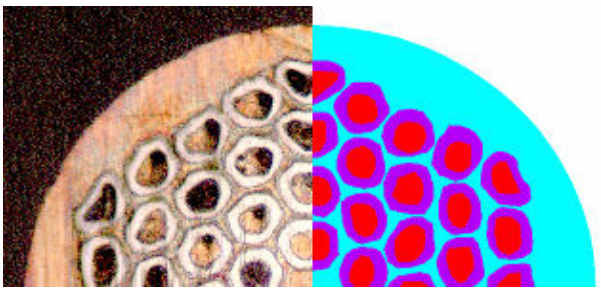

Fig. 2. The actual geometry of the RRP2 strand and the finite element model. Strand diameter is 0.7 mm.

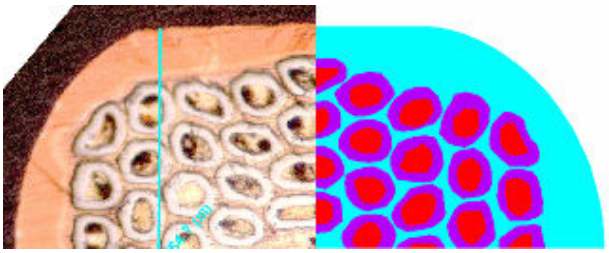

Fig. 3. The actual geometry of the RRP2 strand and the finite element model. Strand depth is 0.55 mm.

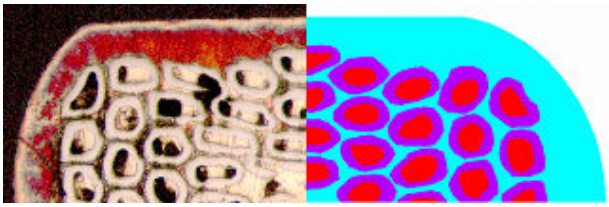

Fig. 4. The actual geometry of the RRP2 strand and the finite element model. Strand depth is 0.5 mm.

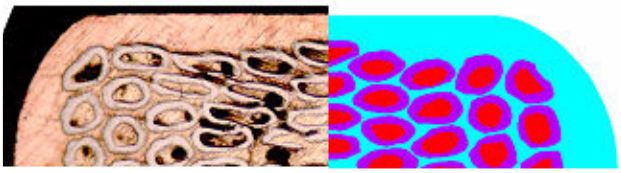

Fig. 5. The actual geometry of the RRP2 strand and the finite element model. Strand depth is 0.45 mm.

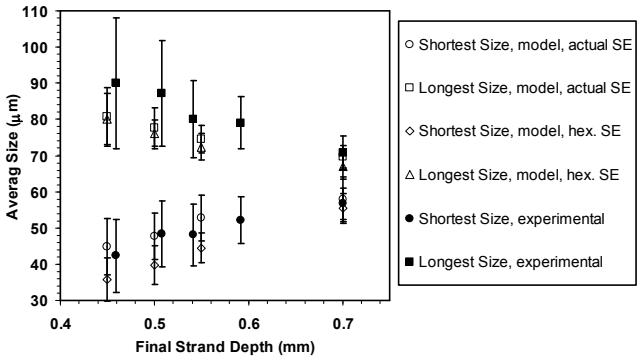


Fig. 6. Comparison of the longest and shortest sub-element sizes between the measurements and the numerical calculations for RRP2.

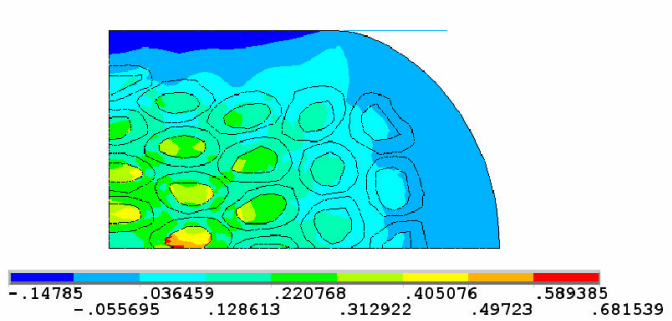


Fig. 7. Strain-x for the RRP2 strand. Strand depth is 0.45 mm.

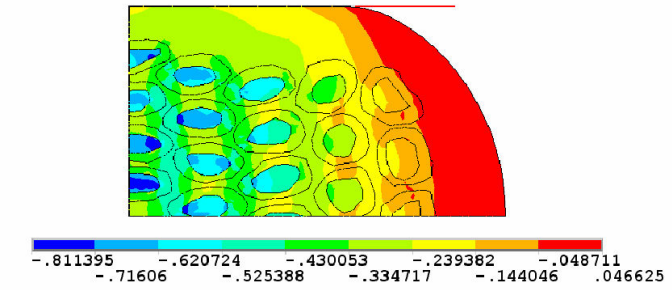


Fig. 8. Strain-y for the RRP2 strand. Strand depth is 0.45 mm.

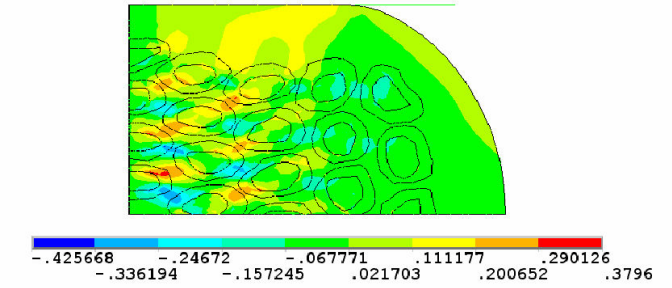


Fig. 9. Strain-xy for the RRP2 strand. Strand depth is 0.45 mm.

## IV. Results

To study the effect of Cu spacing between the sub-elements on the strain values, a 1 mm 120/127 strand was modeled for three cases: regular spacing, represented by a local Cu-to-non-Cu ratio of 0.11 as in the RRP3 strand, 50% increased spacing, represented by a local Cu-to-non-Cu ratio of 0.165 as in the RRP2 strand, and 100% increased spacing. Hexagonal sub-elements were used. Fig. 10 shows the geometry with the array of sub-elements for the 120/127 strand with 50% increased spacing. All the models were subjected to 10%, 20%, and 30% relative deformation. Figs. 11, 12, and 13 show the strain components at 30% deformation level. The maximum strain components were recorded at each deformation stage. Fig. 14 shows the maximum strain components as a function of the relative deformation. One can see that while the shear strain appears to increase linearly with strand deformation, strain x and strain y increase faster. Fig. 15 shows the maximum strain components as a function of Cu spacing between the sub-elements at 20% and 30% deformation levels. At 30% deformation level, the strain component to benefit most from the Cu spacing increase is the shear strain.

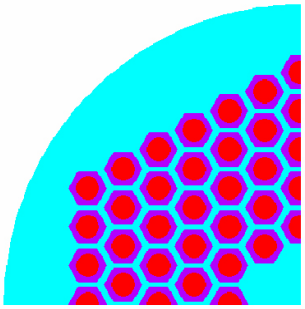

Fig. 10. The 120/127 strand with hexagonal sub-elements and 50% increased spacing. Diameter is 1 mm.

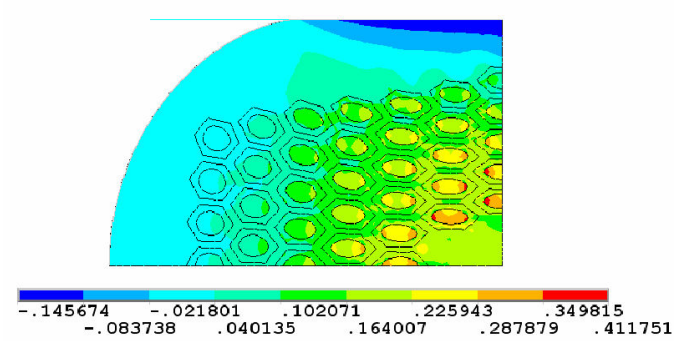


Fig. 11. Strain-x for the 120/127 strand with 50% increased spacing. Strand depth is 0.7 mm.

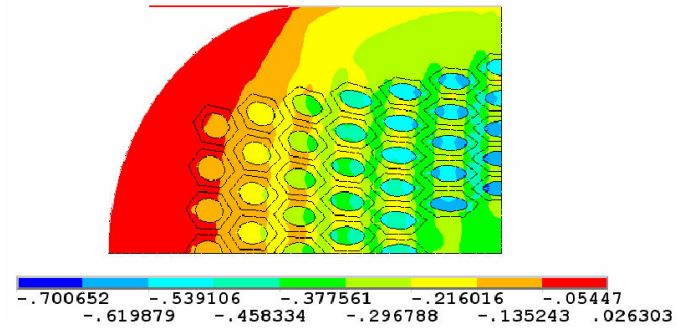


Fig. 12. Strain-y for the 120/127 strand with 50% increased spacing. Strand depth is 0.7 mm.

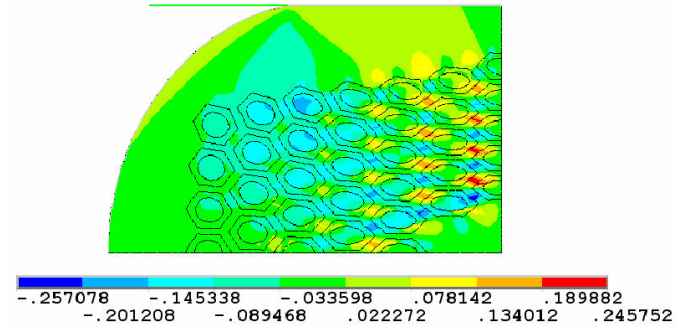


Fig. 13. Strain-xy for the 120/127 strand with 50% increased spacing. Strand depth is 0.7 mm.

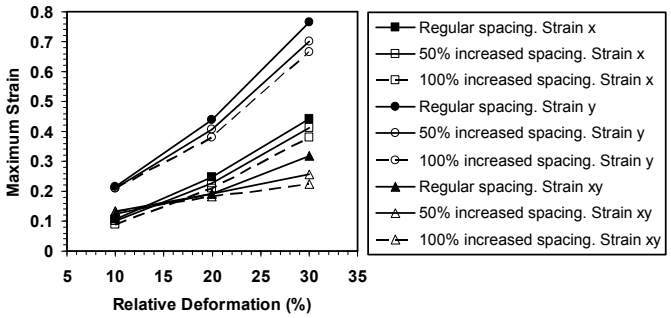


Fig. 14. Maximum strain components as a function of relative deformation for the 120/127 strand. Three cases of Cu spacing between the sub-elements were considered: regular spacing (local Cu-to-non-Cu ratio of 0.11), 50% increased spacing, and 100% increased spacing.

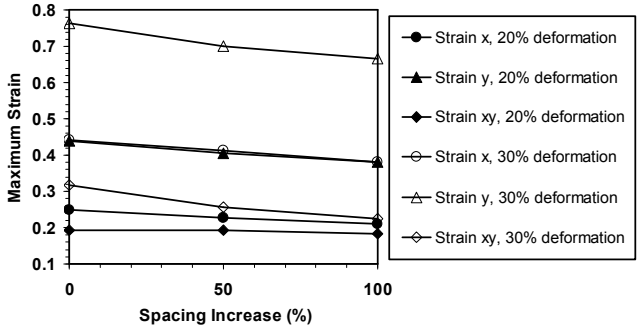


Fig. 15. Maximum strain components as a function of Cu spacing between the sub-elements for the 120/127 strand.

To study the effect of the number of sub-elements on the strain values, 1 mm strands with 54/61, 120/127, and 210/217 arrays were modeled over a deformation range up to 30%. All had a local Cu-to-non-Cu ratio of 0.165. Sub-elements dimensions were determined by keeping the total ratio of niobium to Cu constant in the cross section. Fig. 16 shows the maximum strain components as a function of relative deformation.

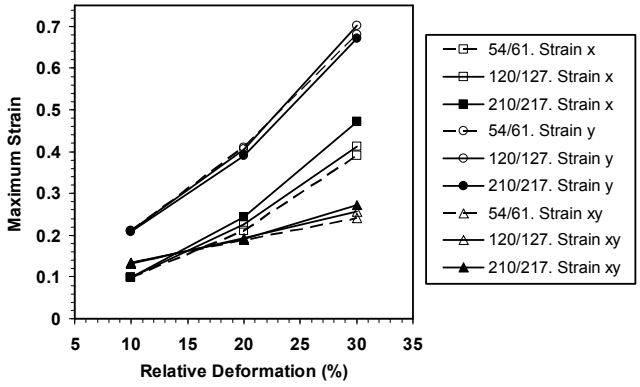


Fig. 16. Maximum strain components as a function of relative deformation for the 54/61 strand, 120/127 strand, and 210/217 strand. All had a local Cu-to-non-Cu ratio of 0.165.

## V. Discussion and Conclusion

The structural finite element modeling of the $Nb_3Sn$ strands, subjected to compressive loads, is effective in predicting the deformed shape of the strands and the sub-elements before fracture or merging of the sub-elements as shown in Figs. 2 to 5. Correlating the finite element results to the experimental images gives the strain values corresponding to fracture of sub-elements. For instance, Figs. 3 to 5 and 7 to 9 show that a strain value of 0.81 causes severe fracture in the sub-elements. This is a numerical-experimental approach that can be implemented to predict failure of sub-elements of this particular strand design.

Increasing Cu spacing between the sub-elements for the 120/127 strand design by 100% reduces the maximum strain-x, maximum strain-y, and maximum strain-xy by 14%, 13%, and 29% respectively at 30% deformation level as shown in Fig. 15. Increasing the number of elements from 54 to 210 sub-elements affects the strain components differently as shown in Fig. 16. It increases the maximum strain-x by 21% and maximum strain-xy by 13%, and it has negligible effect on the maximum strain-y. The change in the maximum strain is due to the structural properties of the sub-elements and especially the tin, which has a smaller stiffness.

The maximum strain components are always located in the sub-elements that are close to the center of the strands as shown in Figs. 7 to 9 and 11 to 13. This agrees with the experimental results.

## Acknowledgment

M. Alsharo'a thanks Muons, Inc. team for the support and continuous collaboration and Mr. Maen Alkhader for useful discussions on the plastic deformation results of $Nb_3Sn$ strands.

## References

[1] D. Turrioni, E. Barzi, M. Bossert, V. V. Kashikhin, A. Kikuchi, R. Yamada, and A. V. Zlobin, "Study of effects of deformation in $Nb_3Sn$ multifilamentary strands," *IEEE transactions on applied superconductivity*, vol. 17, no. 2, June 2007, pp 2710-2713.

[2] S. Farinon, T. Boutboul, A. Devred, P. Fabbricatore, D. Leroy, and L. Oberli, "Finite element model to study the deformations of Nb3Sn wires for the Next European Dipole (NED)," *IEEE transactions on applied superconductivity*, vol. 17, no. 2, June 2007, pp 1136-1139.

[3] E. Barzi, R. Bossert, S. Caspi, D. R. Dietderich, P. Ferracin, A. Ghosh, and D. Turrioni, "RRP $Nb_3Sn$ strand studies for LARP," *IEEE transactions on applied superconductivity*, vol. 17, no. 2, June 2007, pp 2607-2610.

[4] E. Barzi, D. Turrioni, R. Yamada, A. V. Zlobin, M. Alsharo'a, J. Parrell, M. Field, S. Hong, and Y. Zhang, "Effect of subelement spacing in RRP $Nb_3Sn$ strands," submitted to 2007 Cryogenic Engineering Conference (CEC) and International Cryogenic Materials Conference (ICMC), July 2007.

[5] ANSYS, Inc. www.ansys.com.

[6] *Atlas of stress-strain curves*, 2nd ed. The Materials information society-ASM International, Materials Park, OH.

# A SIX-DIMENSIONAL MUON BEAM COOLING EXPERIMENT*

M. A. C. Cummings#, R. P. Johnson, M. Alsharo'a, M. Kuchnir,
K. Paul, T. J. Roberts, Muons Inc., Batavia, IL 60510, U.S.A.
V. Kashikhin, V. Yarba, K. Yonehara, FNAL, Batavia, IL 60510, U.S.A.
D. M. Kaplan, IIT, Chicago, IL 60616, U.S.A.

*Abstract*

Ionization cooling, a method for shrinking the size of a particle beam, is an essential technique for the use of muons in future particle accelerators. Muon colliders and neutrino factories, examples of such future accelerators, depend on the development of robust and affordable ionization cooling technologies. A 6D cooling experiment has been proposed, incorporating a novel configuration of helical and solenoidal magnets in a prototype cooling channel. This Helical Cooling Channel (HCC) experiment is being designed to provide an affordable and striking demonstration that 6D muon beam cooling is understood well enough to enable intense neutrino factories and high-luminosity muon colliders. Because of the large amount of expected beam cooling, helium instead of hydrogen can be used for the initial experiment, avoiding the safety complications of hydrogen. The main points of the experiment are described and corresponding numerical simulations are reviewed.

## INTRODUCTION

Ionization cooling is the only technology that can rapidly reduce muon beam emittances [1] before acceleration. This technique uses energy absorption via ionization loss with RF acceleration to restore the longitudinal momentum within a strongly focusing magnetic lattice to increase the particle density in transverse phase space. Multiple scattering in the absorber introduces "heating" that competes with the ionization "cooling", leading to the choice of a low Z material for the absorber. Liquid or gaseous hydrogen optimizes the heating/cooling trade-off, though safety concerns make engineering such cooling channels a significant challenge.

This technique only reduces the emittance in the transverse directions. In order to cool the six dimensional (6D) emittance of a beam, longitudinal emittance must be transferred to transverse emittance where ionization cooling is effective. This "emittance exchange" had been accomplished in earlier cooling schemes by introducing dispersion via a dipole and directing the higher momentum muons through more ionization energy loss in a wedge-shaped absorber. The idea of pressurized RF cavities [2,3], described elsewhere in this conference, led to the concept of a cooling channel filled with a continuous homogeneous absorber, that exploits the path length (and therefore energy loss) correlation with momentum in a magnetic channel with positive dispersion, such that the momentum spread of the beam is reduced. Since dispersion spreads the beam transversely, the transverse emittance is increased. The usual ionization cooling then acts on the transverse emittance for 6D cooling. Figure 1 depicts the old and new concepts for emittance exchange.

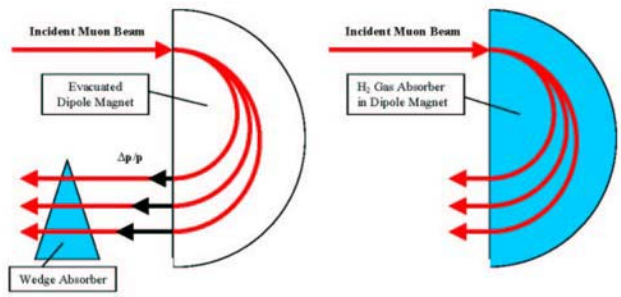


Figure 1: Emittance exchange: the use of a wedge absorber is shown at left, compared with the use of a continuous absorber (right).

The experiment we will propose exploits the emittance exchange concept by using a 4 meter long Helical Cooling Channel (HCC) [4], and measuring its beam cooling properties. This experiment will require a 300 MeV/c muon beam line equipped with up and downstream matching sections, particle spectrometers, and particle identification detectors. The expected cooling factor of nearly 500% will be a striking demonstration of a new technique to cool all dimensions of a muon beam in a time much shorter than the muon lifetime.

## HELICAL DIPOLE MAGNET

The emittance exchange described above is accomplished in the HCC by superimposing a transverse helical dipole magnet and a solenoidal magnet with a continuous absorber medium. The helical dipole magnet creates an outward radial force due to the longitudinal momentum of the particle while the solenoidal magnet creates an inward radial force due to the transverse momentum, or

$$\begin{aligned} F_{h-dipole} &\approx p_z \times B_\perp; \quad b \equiv B_\perp \\ F_{solenoid} &\approx -p_\perp \times B_z; \quad B \equiv B_z \end{aligned} \tag{1}$$

where $B$ is the field of the solenoid, the axis of which defines the $z$ axis, and $b$ is the field of the transverse helical dipole at the particle position. In the HCC described above, RF cavities restored the longitudinal

* Supported by USDOE contract DE-AC02-76CH03000 and grants DE-FG02-03ER86191 and -03ER83722
#macc@muonsinc.com

momentum, and the fields were kept constant. However, in the case where the muon momentum is decreasing through material with no compensating RF, the fields can be adjusted to maintain a stable orbit. The solution for a particle in a HCC with period $2\pi/k$ on an equilibrium orbit with radius $a$ and momentum $p$ can be written:

$$p(a) = \frac{\sqrt{1+\kappa^2}}{k}\left[B - \frac{1+\kappa^2}{k}b\right] \qquad (2)$$

where $\kappa = ka = p_\perp / p_z$ is the arctangent of the helix pitch angle at the periodic orbit, This relationship can be exploited to accommodate a muon beam losing momentum to ionization in a continuous medium to provide the required dispersion and orbit for effective cooling.

Equation (2) shows how to manipulate field parameters to maintain stability for cases where one would like the momentum and/or radius of the equilibrium orbit to change for various purposes [5]. Examples of these purposes that we have examined include a continuous-absorber precooler, a transition section between two HCC magnet sections with different diameters, and an alternative to the original HCC filled with pressurized RF cavities using liquid-filled HCC sections alternate that with evacuated RF cavities. Figure 2 shows a simulation of a decay channel using HCC-type magnets leading to a HCC precooler.

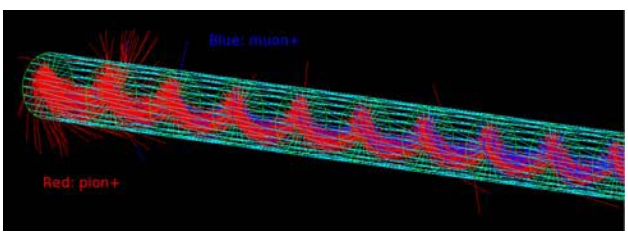


Figure 2. One application of the HCC-type magnet: pion decay channel upstream of the first stages of muon cooling (red tracks are pions, blue tracks are muons).

## 6D MUON AND NEUTRINO EXPERIMENT (6DMANX)

In 6DMANX, we will demonstrate the use of a HCC with a continuous homogeneous absorber to achieve emittance exchange and 6D cooling. This demonstration simplifies the cooling technique by leaving out the RF cavities altogether. Implicit in this approach is that the experiment need only demonstrate the reduction of the invariant normalized emittance. To avoid the need for thick windows, we will use liquid, rather than high-pressure gas. To avoid safety complications, we will use helium instead of the optimal hydrogen. In addition, equation (2) allows us to design decreasing magnetic fields to maintain an equilibrium orbit as the muons lose momentum.

There are several goals we wish to achieve by this experiment to demonstrate:

1) Emittance exchange and longitudinal cooling,
2) 6D cooling in a continuous absorber,
3) Helical Cooling Channel theory and technology,
4) Practical ionization cooling,
5) A prototype precooler,
6) A prototype of one of ~10 HCC sections alternating with RF sections to get $10^6$ 6D emittance reduction.

We propose to run this as a single-particle experiment, with the position, momentum and time of each muon traversing the HCC reconstructed offline before and after cooling. The muon beam enters an upstream spectrometer which measures the particle trajectories. A matching section, which can be integrated with the spectrometer, then brings the beam to match the HCC acceptance. The beam then passes through a thin window that contains the liquid helium of the HCC. The beam passes through the liquid helium-filled HCC in which the momentum is decreased and 6D cooling occurs. The ~150 MeV/c beam exits the HCC through another thin window into the downstream matching and spectrometer sections and is stopped in a calorimeter. Timing and Cherenkov counters upstream of the spectrometer sections and the calorimeter at the end of the channel will be used for particle identification.

Muon bunches are selected and reconstructed offline, and the normalized emittances are calculated from the trajectory and momentum information from the spectrometers to measure the cooling. A simple schematic is presented below in Figure 3.


Figure 3: Schematic of a 6DMANX experiment.

We have proposed that Fermilab construct the HCC magnet(s) and help determine the most expedient location for the experiment. The parameters of the 4 meter helical dipole magnet for a possible 6DMANX HCC are presented in Table 1. Further studies may yield refinements that can reduce costs or enhance performance. The orbits and apertures may have to be tuned to accommodate different experimental configurations.

One possibility we are considering is to place a HCC magnet between the MICE (Muon Ionization Cooling Experiment) spectrometers in the ISIS beamline at Rutherford Appleton Laboratory (Fig. 4).

Table 1: Nominal 6DMANX Parameters

| **Helical Magnet** | **z = 0 m** | **z = 4 m** |
|---|---|---|
| Total length | 4 m | |
| Magnet bore diameter | ~0.8 – 1.0 m | |
| Helix period | 2 m | |
| $\kappa$ (atan of helix pitch angle) | 0.8 | |
| *B* (solenoid) on ref. orbit | -4.4 T | -2.2 T |
| *b* (dipole) | 0.95 T | 0.45 T |
| *b'* (quadrupole) | 0.60 T/m | 0.40 T/m |
| *b"* (sextupole) | -0.26 T/m$^2$ | - 0.15 T/m$^2$ |
| **Beam** | | |
| Beam momentum | 300 MeV/c | 150 MeV/c |
| Beam diameter | 20 cm | |
| Beam $\Delta p/p$ | +/-7% | |

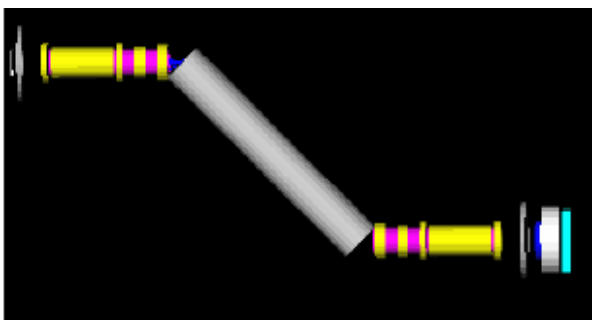

Figure 4: One possible configuration of 6DMANX (HCC in gray) is shown in a GEANT4 simulation using the MICE spectrometers in the RAL ISIS beamline.

Figure 5 shows the normalized transverse (the average radial and azimuthal), longitudinal, and 6D emittances plotted as a function of the distance down the 4 meter HCC. The settings of the helical dipole, helical quadrupole and solenoidal magnets are chosen to give equal cooling decrements in all three planes. The combined 6D cooling factor is about 5.4, corresponding to 1.7 coming from each of the three planes.

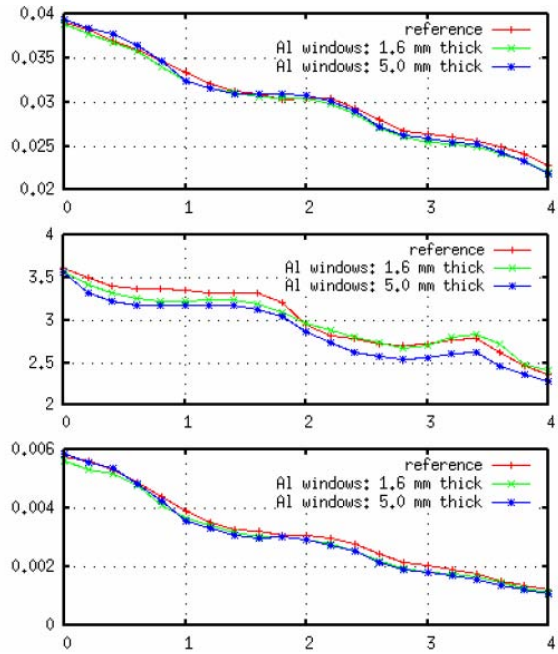


Figure 5: Cooling performance. Shown are the results of simulations (including the effects of windows) of the transverse (top), longitudinal (middle) and 6D (bottom) emittances in the 6DMANX HCC. The axes are emittance (m rad) vs. length of cooling channel (m).

The design of the 6DMANX cryostat for liquid helium can be adapted for a real cooling channel using liquid hydrogen. The very small emittances achievable through such cooling techniques will enable high luminosity for muon colliders [6] and perhaps high intensity for neutrino factories [7]. The small emittances solve many problems for muon colliders: neutrino radiation, decay electrons in detectors and magnets, proton targetry, and heating of the energy absorbers. With enhanced cooling techniques, a muon beam could be quickly cooled to fit into the small apertures of ILC-type RF cavities, reviving the idea of an energy frontier muon collider.

## REFERENCES

[1] Daniel M. Kaplan, "Introduction to Muon Cooling", http://www.slac.stanford.edu/econf/C010630/papers/M102.PDF.
[2] Rolland P. Johnson and Daniel M. Kaplan, http://www-mucool.fnal.gov/mcnotes/public/pdf/muc0195/muc0195.pdf
[3] P. Hanlet et al., these proceedings.
[4] K. Yonehara et al., these proceedings
[5] Y. Derbenev and R. P. Johnson, Phys. Rev. ST Accel. Beams 8, 041002 (2005).
[6] K. Paul et al., Summary of the Low Emittance Muon Collider Workshop, these proceedings.
[7] M. Popovic et al., these proceedings.

# HIGH FIELD SOLENOID MAGNETS FOR MUON COOLING

S. A. Kahn#, M. Alsharo'a, P. Hanlet, R. P. Johnson, M. Kuchnir,
D. Newsham, Muons Inc., Batavia, IL 60510, U.S.A.
R.C. Gupta, R.B. Palmer, E. Willen, BNL, Upton, NY 11973, U.S.A.

*Abstract*

Magnets made with high-temperature superconducting (HTS) coils operating at low temperatures have the potential to produce extremely high fields for use in accelerators and beam lines. The specific application of interest that we are proposing is to use a very high field (of the order of 50 Tesla) solenoid to provide a very small beta region for the final stages of cooling for a muon collider. With the commercial availability of HTS conductor based on BSCCO technology with high current carrying capacity at 4.2 K, very high field solenoid magnets should be possible. In this paper we will evaluate the technical issues associated with building this magnet. In particular we address how to mitigate the high Lorentz stresses associated with this high field magnet.

## INTRODUCTION

Previous studies on the requirements of a muon collider have shown that substantial phase space reduction will be needed in order to achieve the desired luminosity [1, 2]. In order to achieve the luminosity of $7\times10^{34}$ for a 3 TeV center of mass energy muon collider a 6D phase space reduction by $10^6$ may be necessary. A number of muon cooling approaches have been investigated. A simulation of a cooling channel using helical dipole magnets for dispersion and gaseous $H_2$ as an absorber has shown a phase space reduction factor of 50,000 [3]. Further cooling can be achieved using parametric resonance ionization cooling (PIC) along with reverse emittance exchange [4]. 50 Tesla magnets can play a role providing cooling before entering the PIC cooling channel or as a final stage of muon cooling. This cooling stage could be an alternating solenoid lattice where a liquid $H_2$ absorber is placed in the center of a high field solenoid. The minimum emittance that can be achieved is that which occurs when the ionization cooling is balanced by heating from multiple scattering. This minimum transverse emittance is given by

$$\min \varepsilon_{xN} = \frac{\beta_\perp E_s^2}{2\beta_v mc^2 L_R \left|\frac{dE}{dz}\right|}$$

where $\beta_v$ is the muon velocity, $\left|\frac{dE}{dz}\right|$ is the energy loss along the muon path and $\beta_\perp$, the transverse beta function, is given by $\beta_\perp = \frac{2p_z}{cB_z}$. The minimum emittance occurs where $\beta_\perp$, is minimum and the larger the field of the solenoid, the smaller the $\beta_\perp$ that can be achieved.

#kahn@muonsinc.com

This paper will examine how to achieve a solenoid magnet with a field 40-50T using high temperature superconductor that is currently available commercially. This is a concept study that is concerned with how to achieve the field while containing the Lorentz forces.

## MAGNET DESCRIPTION

The choice of the physical dimensions is dictated by the muon cooling requirements. By design the muon kinetic energy entering the solenoid is ~60 MeV which determines that length of the solenoid should be 70 cm. The inner radius of the solenoid is determined by the minimum bending radius of the conductor, but it is consistent with the size of the liquid hydrogen absorber vessel needed for the muon beam.

### *Conductor Choice*

HTS conductor was chosen over $Nb_3Sn$ or NbTi superconductor because it can carry significant current in the presence of high fields. Fig 1 shows the critical current, $J_c$, as a function of field for NbTi, $Nb_3Sn$, and BSCCO 2212 wire [5]. For fields above 14 Tesla, the HTS wire has the greatest current carrying capability. In this study we are using BSCCO 2223 HTS tape from American Superconductor (ASC) [6] instead of the BSCCO 2212 wire, which has a larger current density, because the tape is currently available commercially with documented specifications and is available in a variety that is reinforced to be able to withstand high tensile strain.

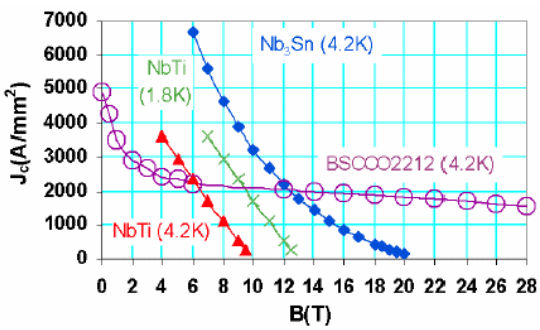


Fig 1: Critical current as a function of field for NbTi, $Nb_3Sn$ and BSCCO 2212.

Table 1 lists the important properties of this conductor used in the study. In addition ASC supplied the data on $J_e$ at 4.2°K, which is shown in fig 2 as a scale factor to be multiplied by the current density at 77° K. The two curves show that the $J_e$ is sensitive to the direction of the field with respect to tape orientation. It was necessary to make an extrapolation from these data to high field, which

introduces some uncertainty in the calculations made. In this analysis we will assume that we are operating at 85% of the maximum critical current. Since development of improved HTS conductor is expected in the future, the choice of which conductor is most appropriate should be revisited.

Table 1: Properties of American Superconductor High Strength Plus Wire

| **Parameter** | **High Strength Plus Wire** |
|---|---|
| Engineering Current Density, $J_e$ | 133 amp/mm$^2$ |
| Thickness | 0.27 mm |
| Width | 4.2 mm |
| Maximum Tensile Strength | 250 MPa |
| Maximum Tensile Strain | 0.4 % |
| Minimum Bend Radius | 19 mm |
| Maximum Length | 400 m |

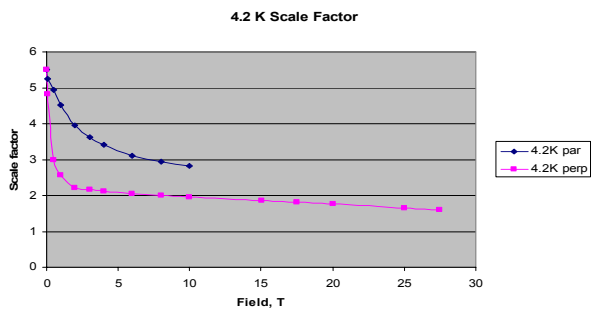


Fig 2: Scale factor to be multiplied by the 77°K current density for the American Superconductor HTS wire used. The blue (magenta) curve corresponds to the parallel (perpendicular) field orientation.

## *Mechanical Choices*

Constraining the large Lorentz forces is the major design concern of very high field magnets. In this study we are proposing to mitigate the build-up of Lorentz forces by interleaving stainless steel tape under tension between the layers of the HTS tape. The interleaved stainless steel will prevent the HTS tape from exceeding its maximum tensile strain limit. We have examined cases with a fixed thickness stainless steel interleaving and with interleaving thickness varied to give the maximum allowable strain at each turn to minimize the amount of superconductor required.

Fig 3 shows strain vs. radius curves for a 40 Tesla solenoid with various thicknesses of stainless steel interleaving. The tensile strain is not maximum at the inner radius where the Lorentz stress is large. Since it comes from the hoop stress of the interleaving and conductor tape, it grows with radius giving a maximum value near the center of the magnet. This is advantageous since there is an additional contribution to the strain from the bend of the HTS tape at small radius. Figure 3 indicates that the smallest stainless steel interleaving thickness that keeps the conductor strain less than 0.4% is 5 mils. A 40 Tesla magnet constructed in this manner (case 1) would have an outer radius of 20 cm. Using this same approach for a 50 Tesla solenoid would require a 13 mil stainless steel interleaving which would significantly increase the outer radius of the magnet and consequently the amount of HTS needed.

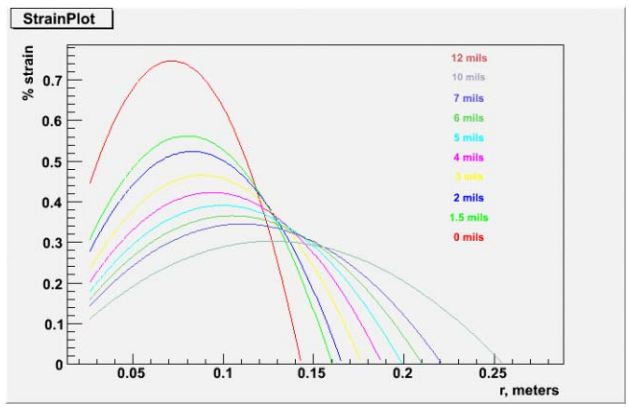


Fig 3: Tensile strain on the HTS conductor as a function of radial position for various thicknesses of stainless steel interleaving in a 40 Tesla solenoid.

The second approach is to vary the stainless steel interleaving thickness on each turn so as to have the largest current density such that the strain on the HTS tape does not exceed the maximum allowable tensile strain limit. The current density varies as a function of radius. This approach was applied to both a 40 Tesla (case 2) and a 50 Tesla (case 3) solenoid. The physical properties of these cases are listed in Table 2. The variable thickness model is more efficient in the use of the superconductor tape, however the magnet is under maximum strain throughout. In addition, by using separate power supplies, one can increase the current density as a function of radius since the solenoid field falls off with radius.

Table 2: Parameters describing the physical properties of the three cases examined.

| Parameter | Case 1 | Case 2 | Case 3 |
|---|---|---|---|
| Stainless Steel width | 5 mil fixed | variable | variable |
| $B_0$ tesla | 40 | 40 | 50 |
| Inner Radius, mm | 25 | 25 | 25 |
| Outer Radius, mm | 200 | 168 | 224 |
| Conductor Length, km | 60.0 | 46.7 | 59.9 |
| Current, mega-amp-turns | 23.56 | 23.20 | 29.73 |

## MAGNETIC PROPERTIES

These three cases were modeled using the OPERA-2D finite element program [7]. It is assumed in these calculations that the solenoid is 70 cm long. Table 3 shows the magnetic properties from the analysis. Since these magnets have significant stored energy, a quench protection system will be necessary to dissipate the energy safely in case of an incident. As expected, the table also shows large radial forces which are mitigated locally so they do not accumulate. There are also compressive axial forces present from the radial fields at the ends of the magnet. Fig 4 shows the axial force density at the end of the magnet as a function of radius for the three cases. Fig 5 shows the axial force density along the magnet length for the radius where the force density is maximal. The allowable compressive strain that the HTS tape can tolerate is less than 0.15%. In the end region it may be necessary to reinforce the conductor against this compressive force. In the end region the HTS conductor can be wound as *pancakes* with stainless steel foil of appropriate thickness to prevent this compressive force buildup.

Table 3: Parameters describing the magnetic properties of the three cases examined.

| Parameter | Case 1 | Case 2 | Case 3 |
|---|---|---|---|
| Stainless Steel width | 5 mil fixed | variable | variable |
| $B_0$, tesla | 40 | 40 | 50 |
| $\int B \cdot dl$, tesla-m | 29.58 | 29.12 | 37.32 |
| Stored Energy, mega joules | 11.0 | 7.8 | 20.5 |
| Total Radial Force, mega newtons | 201 | 173 | 340 |
| Axial End Force, mega newtons | -16.5 | -11.9 | -30.5 |

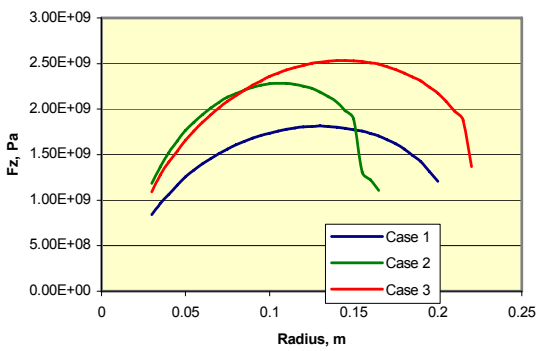


Fig 4: Axial force density along the radius at the end of the magnet for the three cases.

## CONCLUSIONS

Very high field solenoid magnets up to 50 Tesla will play an important role in the final stages of cooling of muon beams for a muon collider. A 45 Tesla solenoid magnet using a Bitter magnet insert has been built at the NHFMF. It has the approximate specifications that would be needed for a muon collider. In this paper we have presented a concept for how a high field solenoid magnet could be build using HTS conductor at 4.2° K.

## ACKNOWLEDGMENTS

This work was performed in part with the support of the US DOE under Contract No. DE-AC02-98CH10886 and in part by Muons Inc. under US DOE SBIR Grant No. DE-FG02-04ER86191.

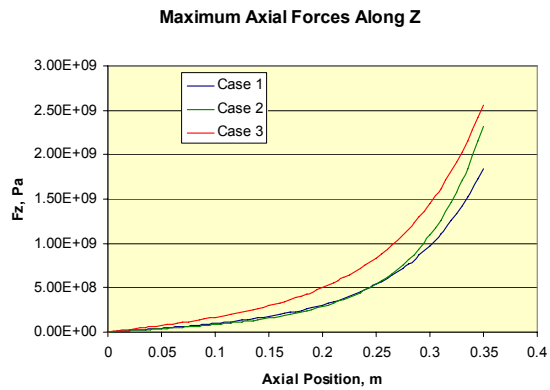


Fig 5: Axial force density along magnet length for each case at the radius where the force density is maximal.

## REFERENCES

[1] C. M. Ankenbrandt et al., "Status of Muon Collider Research and Development and Future Plans", Phys. Rev. ST Accel. Beams **2**, 081001 (1999).

[2] R. P. Johnson et al., "Recent Innovations in Muon Beam Cooling and Prospects for Muon Colliders", Proc. of 2005 Particle Accelerator Conference, Knoxville, p 419.

[3] Y. Derbenev and R. P. Johnson, "Six-Dimensional Muon Cooling Using a Homogeneous Absorber…", Phys. Rev. ST Accel Beams, **8**, 041002 (2005).

[4] Y. Derbenev and R. P. Johnson, "Parametric-resonance Ionization Cooling and Reverse Emittance Exchange for Muon Colliders", COOL05 Presentation, http://www.muonsinc.com/reports/COOL05_PIC_and_REMEX_for_MC.pdf

[5] R. Gupta et al., "R&D for Accelerator Magnets with React and Wind High Temperature Superconductors", Proc of the 17th Intl Conf on Magnet Technology (MT-17), Geneva, (2001).

[6] American Superconductor specification sheet for HTS conductor, http://www.amsuper.com/products/htsWire/documents/WFS_HSP_1205_FINAL.pdf

[7] OPERA-2D is a finite-element suite of programs for electromagnetic design analysis. It is a product of Vector Fields, ltd.